



Reconstruction of Missing Energy Kinematic Events using Forward Tagging at The LHC

Aileene Wang, Ashik Rahman, Gurpriya Dhami, Joe George, Jocelyn
Japnanto, Rishi Kalra, Rishabh Lassen, Swathi Nambiar

Supervisor: Professor Mario Campanelli

University College London
Faculty of Mathematical and Physical Sciences
Department of Physics and Astronomy

Executive Summary

The aim of this project is to improve the accuracy and efficiency of generating W boson directions through a computational kinematic reconstruction. We implement methods proposed by Professor M. Campanelli and doctoral student Y. He, that determined the optimal energy and lepton decay angle parameters to constrain the selection of interaction events from the ATLAS detector at the Large Hadron Collider (LHC).

In the case of the fully leptonic decays of a W boson pair, undetected neutrinos give rise to six unknown parameters due to their neutral charge and negligible mass. The ATLAS Forward Proton (AFP) detector provides momenta measurements of forward protons, which can be used to perform a kinematic reconstruction of the event. The objectives of this project were to improve the code efficiency, optimise the reconstruction parameters and implement a new averaging mechanism to account for multiple W direction solutions. Improved precision of the reconstructed W directions has significance in suppressing combinatorial background, improving sensitivity to the trilinear gauge coupling and providing parameters to further test electroweak theory. The Standard Model Effective Field Theory provides a framework for the fitting procedure in which measurements can be made.

The group approached the project by splitting into theory and computational teams. The theory team researched the physical significance of the reconstruction, forward tagging and the mathematical background of the computational method. The computational team improved the program performance (run-time) by 26%.

An optimal set of energy limit and lepton decay angle limit parameters were also determined using the novel averaging mechanism. This resulted in an optimised energy limit of 11.4 GeV, an angle limit of 0.001335 rad, and 396 azimuthal orientations. These parameters led to a reconstructed W_1 and W_2 angle difference of 46% and 34% closer to zero than initial parameters, respectively. The standard deviations for these differences were 19% lower for W_1 and 6% lower for W_2 . The reconstruction success rate was 96.8%. The effect of proton smearing was also investigated. These results display a significant improvement over the original reconstruction code.

Future research may wish to investigate parallel looping to further improve run-time performance and account for the W mass as a distribution rather than a single value, potentially further improving precision.

Contents

Executive Summary	3
Allocation of Work	3
1 Background	6
2 Theoretical Framework	7
2.1 The Standard Model	7
2.1.1 Fundamental Forces	7
2.2 Physics beyond The Standard Model	8
2.2.1 Standard Model Effective Field Theory	8
2.3 The W Boson	9
2.3.1 W^+W^- Production	9
2.3.2 WW Decay	9
2.4 Special relativity	10
2.4.1 Reference Frames in Special Relativity	10
2.4.2 Lorentz Transformations and Four-Vectors	11
3 The Large Hadron Collider and ATLAS	12
3.1 The Large Hadron Collider (LHC)	12
3.2 The ATLAS experiment	13
3.3 ATLAS Forward Proton (AFP)	14
3.3.1 Experimental Set-up	14
3.4 Experimental Limitations	15
4 WW Kinematic Reconstruction	17
4.1 The WW Reconstruction Algorithm	18
4.2 Code Performance	19
5 Computational Optimisation	22
5.1 Method Overview	22
5.2 Reconstruction Overviews	24
5.2.1 Main Overview	24
5.2.2 Repeated reconstruction overview	26
5.3 Function Overview	28
5.3.1 Loading Data Function	28
5.3.2 Create Directory Function	29
5.3.3 Reference Variables Function	30
5.3.4 Fill Lab Variables Function	31

CONTENTS

5.3.5	WW Boost to Centre-of-Mass Frame Function	31
5.3.6	$W_1 W_2$ Boost to lab Frame Function	33
5.3.7	Get Angle Candidates Function	35
5.3.8	Append Values Function	36
5.3.9	Average Momenta Function	36
5.3.10	Average Opening Angles Function	37
5.3.11	Clear Vectors Function	37
5.3.12	Proton Smearing	38
5.3.13	Average Filter function	39
6	Results & Analysis	43
6.1	Preliminary Findings	43
6.1.1	Energy limit	46
6.1.2	Angle limit	48
6.1.3	Azimuthal increments	50
6.1.4	Optimised results	52
6.1.5	Implementing smearing	54
7	Conclusion	55
7.1	Summary of Results	55
7.2	Further Improvements	56
Acknowledgements		57
Appendix		61
A	Supplementary Code	62
A.1	Header File	62
A.2	Styling File	63
B	Agenda and Minutes	70
C	Finances	87
D	Health and Safety	88
D.1	Risk Assessments	88
D.2	Completion Certificates	90
E	Gantt Chart	99

Allocation of Work

Initials	Full Name	Team
RK	Rishi Kalra	Code
RL	Rishabh Lassen	Code
SN	Swathi Nambiar	Code
JG	Joe George	Code
GD	Gurpriya Dhami	Theory, Code
AW	Aileene Wang	Theory
AR	Ashik Rahman	Theory
JJ	Jocelyn Japnanto	Theory

Table 1: Group Member Team Allocation.

Task	RK	RL	GD	SN	AW	AR	JG	JJ
Literature Review			✓		✓	✓		✓
Executive Summary	✓							
Gantt Chart	✓							
Meeting Minute-Taking		✓						
AFP Detector Research					✓	✓		✓
Particle Physics Research			✓		✓		✓	✓
Computational Research	✓	✓	✓	✓			✓	
Code Optimisation		✓	✓	✓			✓	✓
Code Extensions							✓	
Communications					✓			
Chair for Meetings	✓	✓						
Mid-Term Reviews	✓	✓	✓	✓	✓	✓	✓	✓
Final Report Writing	✓	✓	✓	✓	✓	✓	✓	✓
Final Report Editing	✓	✓	✓	✓			✓	✓
Final Report Formatting	✓	✓					✓	✓
Poster Preparation		✓						✓

Table 2: Task Assignment

CONTENTS

Chapter	Sections	RK	RL	GD	SN	AW	AR	JG	JJ
Executive Summary	<i>Executive summary</i>	✓							
	<i>Team Allocation</i>	✓							
Allocation of Work	<i>Project Allocation</i>	✓							
	<i>Report Allocation</i>	✓	✓						
1. Background	<i>Background</i>	✓							
2. Theoretical Framework	<i>The Standard Model</i>						✓		
	<i>Fundamental Forces</i>						✓		✓
	<i>Beyond The Standard Model</i>						✓		
	<i>The W Boson</i>	✓							
	<i>Special Relativity</i>		✓						
3. The Large Hadron Collider	<i>Large Hadron Collider</i>					✓		✓	
	<i>ATLAS</i>							✓	
	<i>AFP</i>					✓		✓	
4. WW Kinematic Reconstruction	<i>Summary of existing method</i>	✓		✓					
	<i>Event Kinematics</i>	✓	✓	✓					
	<i>Reconstruction Algorithm</i>							✓	
	<i>Code Performance</i>							✓	
5. Computational Optimisation	<i>Method Overview</i>	✓	✓					✓	
	<i>Reconstruction</i>	✓	✓					✓	
	<i>Functions</i>	✓	✓					✓	
6. Results & Analysis	<i>Preliminary Results</i>	✓	✓	✓				✓	
	<i>Analysis</i>	✓	✓	✓				✓	
	<i>Final Results</i>	✓	✓	✓				✓	
	<i>Comparison with original</i>	✓	✓	✓				✓	
7. Conclusion	<i>Conclusion</i>	✓	✓	✓	✓	✓	✓	✓	✓
8. Appendix	<i>Agenda & Minutes</i>		✓						
	<i>Finances</i>	✓	✓						✓
	<i>Risk Assessment</i>	✓	✓						✓
	<i>Completion Certificates</i>		✓						
	<i>Gantt Chart</i>	✓							
	<i>Source Code</i>		✓						
	<i>References</i>	✓	✓	✓	✓	✓	✓	✓	✓

Table 3: Final Report Allocation of Work

Background

The fully leptonic WW boson pair decay presents a difficult task for the reconstruction of kinematic properties due to the six unknown parameters caused by undetected neutrinos. Though kinematic reconstruction of events has been employed for decades in high-energy physics [1][2], the six unknowns in this mechanism mean direct reconstruction is difficult. However, with the precise measurements of two forward momenta by the ATLAS Forward Proton (AFP) detector, constraints on energy and four-momenta may be applied to infer the missing values through computational reconstructive methods. The AFP detects occasions where protons narrowly miss each other, remaining intact and diffracting at small angles, providing initial proton four-momenta to further constrain the system [3]–[5].

Existing code by Prof M. Campanelli and Y. He analysed simulated events from the LHC and reconstructed the W boson direction using an energy cut of 10 GeV, leading to an average angle between reconstructed and truth-level W directions of 0.22 rad, which then becomes 0.25 rad when the proton momentum was smeared to detector level. With this method, an efficiency of 98.3% of candidates passing the cuts was achieved for 1000 events.

Optimisation of candidate selection parameters has been conducted in similar research by the CMS collaboration for the reconstruction of the fully leptonic WZ decay [6] and by A. Ballestrero et al. for the fully leptonic WZ and ZZ channels at the LHC [7]. These involved determining suitable initial parameters, accounting for clusters, and investigating multiple reconstructed solutions. Research by M. Grossi, J. Novak et al. applied deep-learning techniques of kinematic reconstruction for polarisation discrimination in vector boson scattering [8], which may be a potential avenue of extension for this project.

Kinematic event reconstruction for the fully leptonic WW decay allows for the improved sensitivity to trilinear gauge couplings [9]–[11] and suppression of combinatorial background. Enhanced precision in reconstruction is significant in investigating electroweak theory in the TeV regime, electroweak symmetry breaking mechanisms [12][13], Beyond the Standard Model research [14] and Standard Model Effective Field Theory, which are all critical to furthering our understanding of fundamental particle physics. This study proposes an optimised set of parameters and a kinematic reconstruction code for the fully leptonic WW decay, with the aim to support research probing beyond the Standard Model.

Theoretical Framework

2.1 The Standard Model

The Standard Model (SM) [15] of particle physics describes all the currently known fundamental particles and interactions, except for the gravitational force. These particles are elementary and considered to be point-like, hence do not have any internal components or structure. The matter is separated into fermions (half-integer spin particles) and gauge bosons (integer spin particles) [15]. Bosons mediate interactions between fermions. Fermions are categorised into quarks and leptons, and bosons are categorised into scalar and vector, as shown in Fig. 2.1.

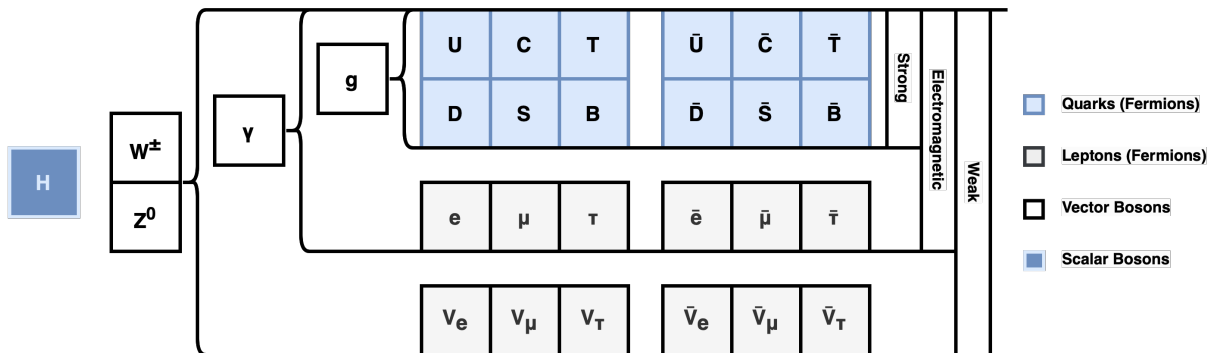


Figure 2.1: A simplified diagram of the Standard Model’s fundamental particles, forces and associated vector boson gauge interactions.

2.1.1 Fundamental Forces

Electromagnetic Interaction

Electromagnetism is responsible for the behaviour of electrically-charged particles and the interaction of electric and magnetic fields. This interaction is mediated by massless photons (γ), which are the particles that form visible light and other types of electromagnetic radiation. In theory, electromagnetic interaction has an infinite range, with its strength inversely proportional to distance.

Strong Interaction

The strong interaction is a confinement theory that confines quarks into protons and other hadrons. The massless gluon (g), which mediates this interaction, carries a colour charge

of either red, green, or blue. There are also six distinct quark flavours: up (u), down (d), charm (c), bottom (b), and top (t). Due to QCD-confinement, these are not observed freely, rather, they are confined as hadrons with net zero colour charge. Due to the gluon carrying colour charge, it is self-interacting, and the resulting strong interaction exhibits a short effective range of the order 10^{-15} m.

Weak Interaction

The weak interaction permits particle flavour violations and is mediated by the W and Z bosons. W bosons are used for charged weak currents and the Z boson for neutral weak currents. The boson itself can also decay. The weak force has an effective range of the order 10^{-17} m.

Electroweak Interaction

Developed in the 1960s, A. Salam et al. [16] proposed a unification of quantum electrodynamics (QED) and the weak interaction as the electroweak force. In high-energy environments, such as the universe less than 10^{-12} s after the Big Bang, the SM describes electroweak interactions occurring through four massless bosons: W_1 , W_2 , W_3 and B . These bosons induced interactions at similar strengths, which is not the case at regular energy levels. Due to spontaneous electroweak symmetry breaking via the Higgs mechanism, which occurs when we go from high to low energies, the bosons mix into the four physical states that are observable in regular interactions: three massive bosons (W^+ , W^- , and Z^0) and one massless boson (γ). The differences in these bosons result in different interactions in which they mediate. The weak interaction is very weak at low four-momentum transfers due to the mediation of the heavy W^\pm and Z^0 bosons. Electromagnetic interactions are stronger because photons are massless. At very high four-momentum transfers, in a case involving a W boson exchange, the scattering amplitude of the interaction is dominated by the intrinsic strength of the interaction rather than the boson mass, and therefore the electromagnetic and weak interactions appear very similar. W and Z bosons were initially required to be massless, like the photon. However, experiments such as the UA1 and UA2 collaborations at CERN [17] have shown these particles to possess mass. The Higgs mechanism rectified this, allowing for a spontaneous break in symmetry when coupling to the Higgs particle, permitting the bosons to have mass without breaking the theory.

2.2 Physics beyond The Standard Model

Despite its success, the SM is not able to account for phenomena such as gravity or dark matter. This suggests the possibility of physics beyond the Standard Model (BSM).

2.2.1 Standard Model Effective Field Theory

One way this is explored is by using the Standard Model Effective Field Theory (SMEFT). This takes a global approach to the SM and allows one to identify small deviations through experiments that could be indicators of BSM physics [14]. In this framework, the SM Lagrangian contains five symmetries and flavour rotations, including lepton and baryon

number, hypercharge, a Peccei-Quinn symmetry, and independent rotations of the right-handed leptons [18]. The Lagrangian requires the use of 6-dimension SMEFT operators. All predictions are made at the parton level, using parton distribution functions (PDFs), with the leading order in perturbation theory.

2.3 The W Boson

The W boson is a very large vector boson with the fourth largest mass in the SM ((80.43 ± 0.01) GeV/c 2) [19]. It has been measured to undergo hadronic decay 67.32% of the time and leptonic decay 32.68% of the time [20].

2.3.1 W^+W^- Production

The W^+W^- pair is produced in the LHC largely via proton-proton collisions [21], where a photon is radiated which then undergoes a quartic gauge coupling to produce W bosons, as shown in Fig. 2.2.

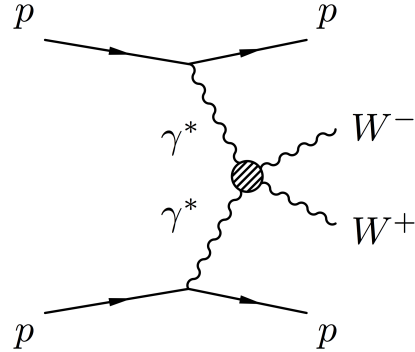


Figure 2.2: Protons radiating photons which produce a W^+W^- pair.

2.3.2 WW Decay

In the SM, the decay channels can be classified into 3 categories as shown in Table 2.1 [22].

Decay Category	Decay Process
Fully Hadronic	$WW \rightarrow q\bar{q}q\bar{q}$
Fully Leptonic	$WW \rightarrow \ell\bar{\nu}_\ell\ell\nu_\ell$
Semi-Leptonic	$WW \rightarrow q\bar{q}\ell\nu_\ell$

Table 2.1: Main methods of WW decay

In the fully leptonic decay, the W^- decays to a lepton (ℓ) and lepton antineutrino ($\bar{\nu}_\ell$). Similarly, the W^+ decays to an antilepton ($\bar{\ell}$) and lepton neutrino (ν_ℓ) as seen in Fig. 2.3.

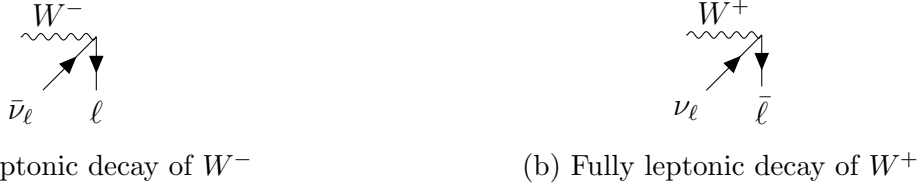


Figure 2.3: Feynman diagrams of the fully leptonic decays of W^- (a) and W^+ (b)

The WW decay is a key process in electroweak theory, thus precise measurements are needed to test the SM's predictions and search for new physics. Hence a high-efficiency reconstruction algorithm is necessary. The significance of reconstructing WW decays lies in SMEFT, where improving sensitivity to trilinear gauge couplings is critical.

2.4 Special relativity

Special relativity [23] is a theory of space-time and provides the best description of the behaviour of objects traveling at near-light speeds, such as particle collisions at the LHC. It is based on the following postulates:

1. The laws of physics are the same in all inertial frames of reference.
2. The speed of light, c , in free space is consistent and the same for all observers, regardless of their motion relative to the source of the light.

Many fundamental concepts are derived from these postulates. One is the relativity of simultaneity, which states that two events that appear simultaneous to one observer may not appear simultaneous to another in relative motion. Another is time dilation states that time appears to pass more slowly for an object in motion relative to an observer at rest. This effect becomes significant at speeds close to the speed of light.

2.4.1 Reference Frames in Special Relativity

Viewpoints or "reference frames" are defined to describe systems relative to that particular frame. An inertial frame is a frame that is stationary or moving at constant velocity, whereas a non-inertial frame is accelerating [24]. There are two types of frames of reference: rest frames and lab frames. A rest frame is a frame in which an object is at rest, while a lab frame is a frame in which an observer is at rest. The lab frame is often used as a reference frame for measuring the motion of objects.

The Center-of-Mass Frame

The center-of-mass (CoM) frame is used in high-energy physics and simplifies the analysis of collisions. By performing calculations in this frame where the CoM is at rest, scattering of N particles can be simplified since the total momentum, P , of particles in the system is zero, so colliding particles have equal and opposite momenta:

$$P = \sum_{i=1}^N p_i = 0 \quad (2.1)$$

2.4.2 Lorentz Transformations and Four-Vectors

The momenta and energy of an object in a particular coordinate system can be written as a vector with four components, i.e. a four-vector:

$$\begin{pmatrix} P_x \\ P_y \\ P_z \\ E \end{pmatrix} \quad (2.2)$$

The scalar product of two four-vectors, i.e. its magnitude, is invariant under Lorentz transformations which transforms the four-vector from one coordinate system to another. The Lorentz matrix allows for such transformations and is given by:

$$\begin{pmatrix} 1 & 0 & 0 & 0 \\ 0 & 1 & 0 & 0 \\ 0 & 0 & \gamma & -\gamma\beta \\ 0 & 0 & -\gamma\beta & \gamma \end{pmatrix} \quad (2.3)$$

where $\gamma = 1/\sqrt{1-\beta^2}$ is the Lorentz factor and $\beta = v/c$ is the ratio of the velocity v of the boosted frame to the speed of light c .

The Lorentz matrix can be applied to transform the four-vector in the S frame to a boosted frame S' moving at v along the z -direction:

$$\begin{pmatrix} P'_x \\ P'_y \\ P'_z \\ E' \end{pmatrix} = \begin{pmatrix} 1 & 0 & 0 & 0 \\ 0 & 1 & 0 & 0 \\ 0 & 0 & \gamma & -\gamma\beta \\ 0 & 0 & -\gamma\beta & \gamma \end{pmatrix} \begin{pmatrix} P_x \\ P_y \\ P_z \\ E \end{pmatrix}, \quad (2.4)$$

where $(P'_x P'_y P'_z E')$ is the transformed four-vector in the S' reference frame.

The Large Hadron Collider and ATLAS

3.1 The Large Hadron Collider (LHC)

CERN's LHC is the world's largest and most powerful particle accelerator. It is a two-ring superconducting hadron accelerator installed in a tunnel of 27 km circumference, 154 m underground in Geneva. The LHC aims to investigate fundamental questions in physics by colliding high-energy particle beams traveling near the speed of light [25]. Fig. 3.1 shows an overview of the LHC complex, which feature other major detectors, including ALICE, CMS, LHCb, and ATLAS [26].

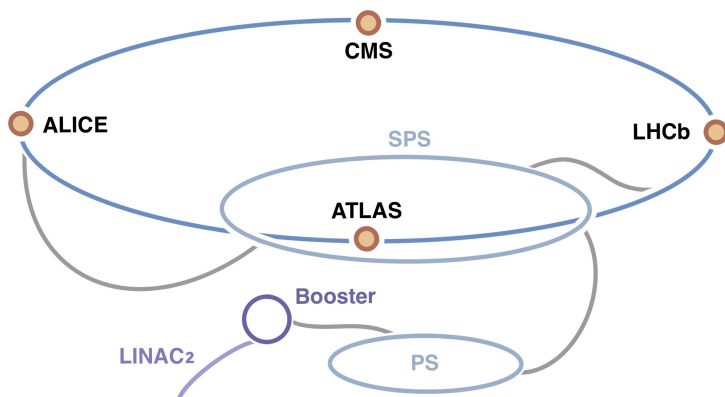


Figure 3.1: Overview of CERN's LHC facility. Adapted from [27].

Protons enter the LINAC2, which fires beams of protons into the Proton Synchrotron (PS) Booster [26]. This uses radio frequency cavities to accelerate the protons and magnetic fields to maintain the track of the beams [28]. The beams then enter the Super Proton Synchrotron (SPS), accelerating further and dividing into bunches of 1.1×10^{11} protons, with 2,808 bunches per beam [29]. The SPS feeds beams into the LHC: one travelling clockwise and the other anticlockwise. Within the LHC, the beams accelerate further before converging at one of the detector sites, resulting in 600,000,000 collisions per second at that position [28][29].

3.2 The ATLAS experiment

ATLAS (**A**Toroidal **L**H_C Apparatu**S**), shown in Fig. 3.2, is the largest general-purpose detector situated at the LHC. Constructed in 2008, it was designed to research physics beyond the SM at a very high TeV scale [30].

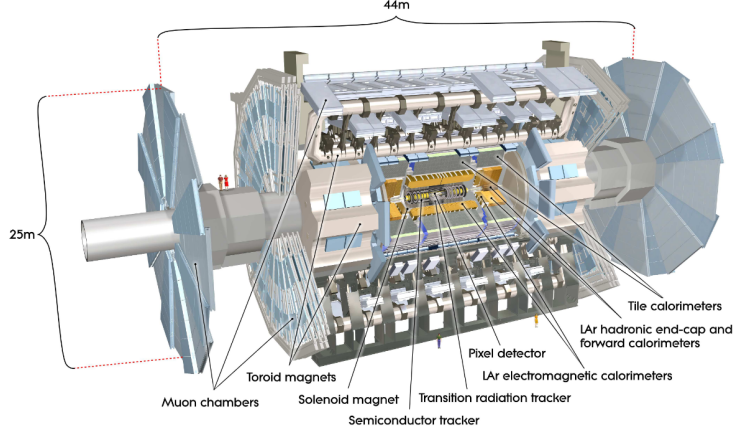


Figure 3.2: ATLAS detector layout including calorimeters and trackers for detection of different types of particles [25].

With the origin set at the interaction point (IP), the z -axis is defined along the beam direction, with the $x - y$ plane set transverse to this. The angle along the $x - y$ plane is given as the azimuthal angle ϕ , while the polar angle θ represents the angle from the beam axis.

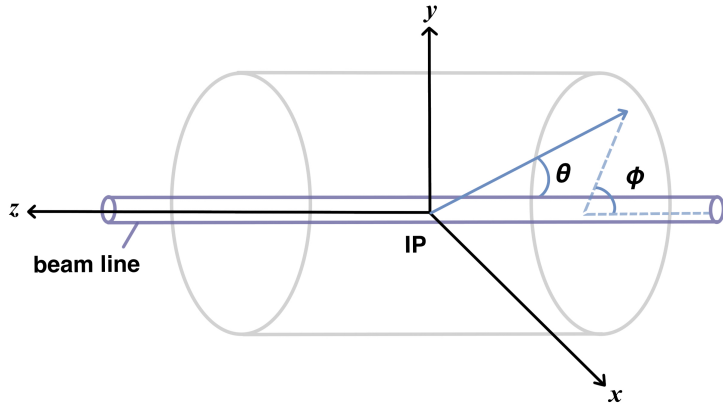


Figure 3.3: Schematic diagram of the ATLAS coordinate system. Adapted from [31].

The scope of ATLAS has been broadened with the addition of four sub-detectors in the forward region [32]: LUCID (LUminosity Cherenkov Integrating Detector), ZDC (Zero Degree Calorimeter), ALFA (Absolute Luminosity For ATLAS), and the most relevant to this project being the AFP (ATLAS Forward Proton).

3.3 ATLAS Forward Proton (AFP)

The AFP project aims to specifically broaden the diffractive physics programme of the ATLAS experiment in the LHC. The LHC primarily detects proton-proton collisions, but an emerging point of interest occurs when these protons narrowly miss one another and remain intact, diffracting at very small angles in a process named Central Exclusive Production (CEP). This process can be generalised with the equation $pp \rightarrow p + X + p$, where X is the central system that may be, for example, a pair of W or Z bosons, a pair of jets, or a neutral Higgs boson [33]. For this to occur, the protons must interact coherently with the emission of a colour singlet object. This interaction can adopt an electromagnetic nature with the exchange of photons or a strong nature with the exchange of Pomerons. In the former case, electromagnetic fields surrounding the protons can interact, leading to high-energy photon-photon interactions and coupling with a lepton pair [4].

Crucially, to investigate these phenomena, the forward protons must be detected by detectors located inside the machine's beampipe. ATLAS initially had a forward detector system installed called the ALFA sub-detector [34], but these were only suitable for detecting elastic scattering during special, low-energy runs. The AFP project recently installed AFP additional detectors that can detect diffractive events during ‘normal’, high-luminosity LHC runs. These conditions give way to testing the electroweak theory at unprecedented precisions.

3.3.1 Experimental Set-up

In the AFP [5], movable beampipes were installed on both sides of the ATLAS experiment. Illustrated in Fig. 3.4, two roman pots are situated symmetrically at ± 205 m (NEAR stations) and ± 217 m (FAR stations) from each side of the IP. The four roman pots all house Silicon Tracker (SiT) planes which precisely measure proton positions. These trackers therefore measure the points along the trajectories of protons that have been deflected from the initial pp collisions. The FAR stations, shown in Fig 3.5, additionally feature time-of-flight (ToF) detectors, which help distinguish relevant signals from pile-up background by precisely measuring the time difference between the two outgoing scattered protons and separating these events from unrelated independent pp collisions.

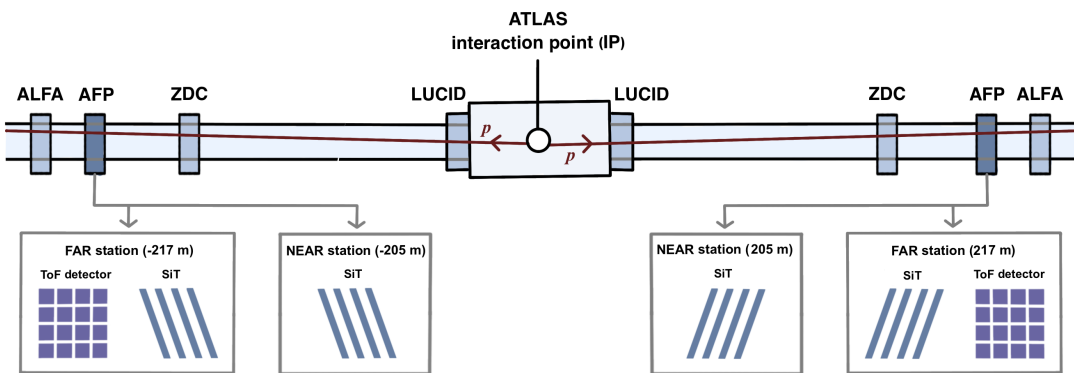


Figure 3.4: Schematic diagram of the AFP detector in ATLAS. The four stations feature Silicon trackers and the FAR stations feature additional time-of-flight detectors.

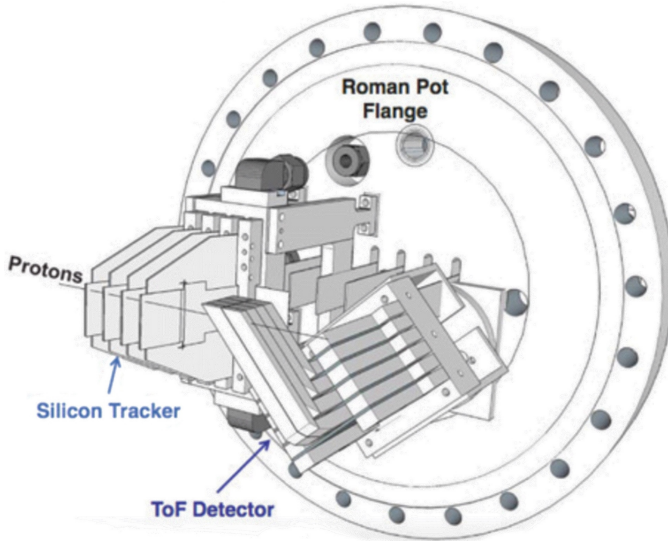


Figure 3.5: Layout of a FAR station in ATLAS [35].

By having a pair of detectors on each side of the IP, the elevation angle of the protons can also be measured in addition to their positions [3]. By measuring the properties of the protons at the detectors, the initial four-momentum can be determined, hence giving insight into the proton kinematics at the IP. Knowing these additional parameters allows for more precise kinematic reconstructions, such as in the case of processes like the WW decay, where not all decay products can be detected. The unprecedented analyses presented by the AFP compared to measurements only taken from the central detector can give profound precision measurements of the electroweak parts of the SM and a possible understanding of electroweak symmetry-breaking mechanisms.

3.4 Experimental Limitations

Boson Path

The boson can only be discovered by creating a particle collision, and will only exist for an extremely short time. Once created, it immediately decays into other particles, meaning the boson path can only be detected by analysing its decay products. Detectors identify the traces of decay products, but these particles can also be produced in other processes. This pile-up background makes determining boson paths more difficult.

Undetectable Neutrinos

Neutrinos are difficult to detect experimentally because they have no electrical charge and very low mass. Since they have no charge, they interact very weakly with other matter, making them undetectable.

As two W bosons decay into two charged leptons and two neutrinos, the leptons are measured by the ATLAS detectors, while the neutrinos are not. Thus the direction of the two neutrinos is missing in the process of reconstructing the full kinematics of the event. For each neutrino that is not observed, there are three momentum components,

and overall six variables are missing.

Six constraints are applied to find the momentum of the neutrinos: the mass of W bosons and four kinematic constraints that include the energy and momentum in the x , y , and z directions due to the conservation of four-momenta.

WW Kinematic Reconstruction

Reconstruction of kinematic events has been employed for several decades, originating in early experiments that studied the properties of the weak force. Examples include the UA1 and UA2 collaborations which measured the masses of the W and Z bosons using decay product energies and angles from proton-antiproton collisions [1][2]. Reconstruction involves applying conservation laws to decay products, such as energy and momentum conservation, and considering the effects of special relativity to reconstruct missing information [36]. This allows properties of decay products that cannot be directly detected to be inferred. More recent research by M. Grossi et al. proposes deep-learning techniques for kinematic reconstruction in vector boson scattering [8], which may be useful for future adaptations of this project and possibly result in efficiency improvements.

Optimisation of traditional reconstruction methods had been conducted by the CMS collaboration for the reconstruction of the fully leptonic WZ decay, which relies on the reconstruction of electrons, muons and the missing transverse momentum associated with the escaping neutrino [20]. The magnitude of the negative vector sum of transverse momenta of all reconstructed candidates was used to calculate this missing energy [20]. Isolation criteria were optimised to match requirements, e.g. the double-electron trigger required two clusters with energy greater than 33 GeV. Similarly, this project will adapt isolation requirements to account for clusters.

In the fully leptonic W boson decay, shown in Fig. 4.1, the escaping neutrino measurements were reconstructed by using the forward tagging applied by the AFP detector, which allows the detection of particles produced at small angles with respect to the beam direction, giving the four-momenta to apply additional constraints on the system.

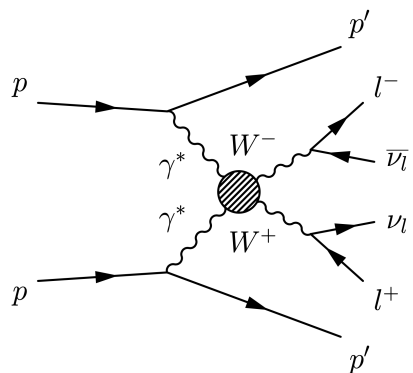


Figure 4.1: Full leptonic decay of the reconstructed event.

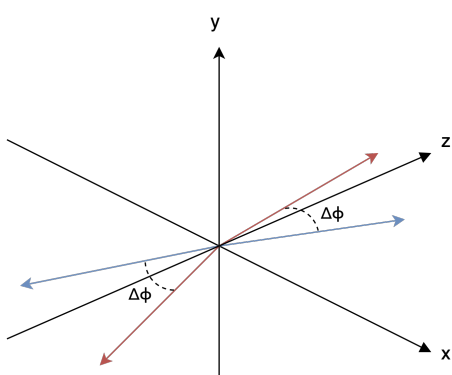
4.1 The WW Reconstruction Algorithm

The original code, written by M. Campanelli and Y. He, employed a numerical approach to reconstruct the W boson direction. This involved constructing four-momenta of the W pairs in the CoM frame of the proton-proton collision, boosting them to the lab frame, and selecting events based on a series of cuts.

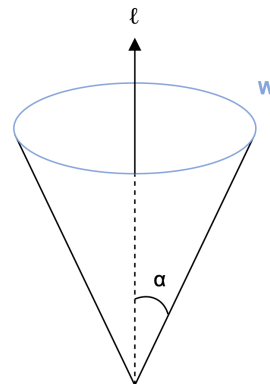
Overview

The reconstruction code followed several key steps:

1. Loading simulated data, these are generated using the Monte-Carlo method
2. Finding the expected four-momenta for the WW system from the simulated data
3. Constructing 1,000,000 kinematic configurations of energy and four-momenta combinations in the WW system's CoM frame
4. Boosting these values to the lab frame for comparison to simulated values
5. Performing an energy cut
6. Calculating the lepton decay angle of these reconstructed W bosons and rotating these in 360 different orientations of their azimuthal angle ϕ with increments $\Delta\phi$ around the beam axis - refer to Fig. 4.2
7. Performing an angle cut
8. Averaging successfully reconstructed momenta to find the final two reconstructed W boson directions.



(a) The WW system in blue is rotated by $\Delta\phi$ to the position in red.



(b) The lepton decay angle α between the lepton ℓ and W directions.

Figure 4.2: Reconstruction event of a fully leptonic WW decay.

4.2 Code Performance

The first limitation identified after testing the code with the default parameters was the extensive code run-time for event evaluation. Therefore, reducing the simulation run-time was prioritised. Code performance was improved via the following steps:

- 1. Re-labelling and removing inconsistent variables
- 2. Restructuring the code
- 3. Substituting techniques with faster alternatives.

Variables

Although seemingly trivial, re-labelling variables provided transparency into the code functionality, allowing for re-usability and comprehension. This was done for the simulation code (`w11.C` file) and output styling code (`dps.C` file).

Redundant variables were also removed. Many required variables were sub-optimally designed and hence improved. For instance, a large number of variables that were implemented for a single use were defined to store inputs as arrays. This was most apparent within the core looping mechanism.

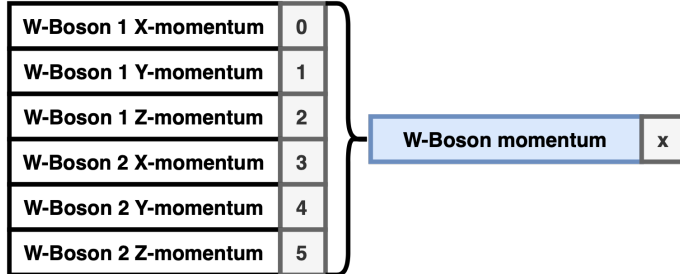


Figure 4.3: Example of a multi-variable reduction into an array.

Inefficient variable definitions were corrected. For example, as particle momenta and energies were often used together, these values were combined into multi-dimensional arrays. This provides easier handling within C++ since contiguous memory locations can be created rather than scattered ones [37]. Additionally, a notable improvement involved the manipulation of reconstructed W bosons, where the momenta frequently undergo the same series of manipulations. These were clustered into two-dimensional arrays with the axis defined by the number of events and another by the six momenta indexed as shown in Fig 4.3. This structure was implemented analogously to other grouped quantities, as it improves clarity, reduces code length, and offers run-time enhancements [37].

Simulation Data

The importing and separation of the Monte-Carlo simulation data into multiple arrays were identified as extremely inefficient. This originally required the manipulation of 24 separate arrays and repeated access to the individual elements at every point called in

the loop. Therefore, this required the system to distribute the information disparately across various memory locations prior to accessing the indexed contents for every repeated event [37][38]. To avoid this, a three-dimensional “carrier” array was introduced to store the loaded quantities prior to unloading them at each successive event. Thus, the entire dataset was imported once into a single array, then the contents were unloaded into individual variables before each event. Therefore, the imported simulation data was handled significantly faster through the loop – since only a single variable is being repeatedly accessed, rather than locating the contents of disparate array elements. This structure is illustrated in Fig. 4.4.

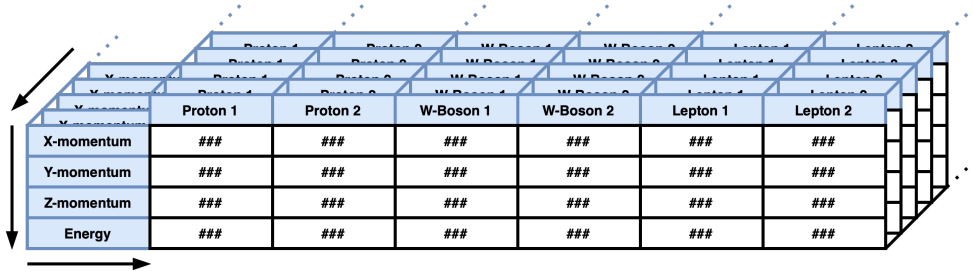


Figure 4.4: Compressed particle data into a three-dimensional array.

Reconstruction

The existing reconstruction mechanism is composed of three independent loops with increasing lengths. These were combined into a single loop, improving the simulation time. Moreover, it improved the looping structure’s legibility and distinguished the relevant cuts in succession. Within this central looping, many arrays were redesigned as single-use variables. For this reason, rather than re-indexing and accessing the corresponding array contents, standard variables were used to perform operations and then reused for subsequent events.

Parallelizing Loops

Conventional loops are one of the main reasons for the elongated run-time. Parallelizing the loops was an effective solution which can be implemented in C++ using *OpenMP* [39], a widely used API that supports parallel programming in shared-memory models.

Parallel loops can execute multiple iterations simultaneously, utilising multiple CPU cores. The addition of a *pragma* statement prior to loop instructs the compiler to execute the loop in parallel. Each thread then executes a subset of the iterations where the number of threads is determined automatically by the system with respect to the available CPU cores.

Typically, for programs that perform complex calculations on large data sets, this process significantly reduces the time needed to execute the loop. However, after implementing these loops, the run-time of the reconstruction code rather increased. This could be due to numerous reasons:

1. Race conditions: when more than one thread attempts to access and modify the shared data at the same time. This results in the order of the thread executions and modifications not being guaranteed, leading to unpredictability and incorrect behaviour.
2. Deadlocks: when a thread is blocked and "deadlocked" with another thread as it requires the other thread's resources to be released to progress. This can occur when threads acquire locks or other synchronisation primitives in a different order.
3. Load imbalance: when the distribution of executions is not uniform which results in some threads being idle while others are overloaded with tasks. This can lead to inefficiencies due to prolonged thread run-times.

In the future, mitigation of such problems could include implementing synchronisation mechanisms such as locks, semaphores, or barriers which control and distribute the access of threads to shared resources. Furthermore, to aid with the detection of these concurrency-related bugs prior to their occurrence, static analysis and dynamic testing tools could be utilised.

Improved Code Performance

In combination, these technical modifications offered significant improvements in code run-time performance. A comparison is shown in Table 4.1.

Trial	Original run-time (ms)	Optimised run-time (ms)
1	77243	57711
2	76458	56184
3	76185	57798
4	77639	57946
5	78149	56611
Average	77134.8	57250

Table 4.1: Run-time comparison of original and optimised code for 50 events subject to default parameters.

Here we find that for the optimised code set to the default parameters and 50 reconstruction events, our program is 26% more efficient than the original program on average. This was even performed using the optimised code containing additional functions and mechanisms.

Computational Optimisation

5.1 Method Overview

An outline of the most fundamental components of the optimised program is illustrated in Fig 5.1.

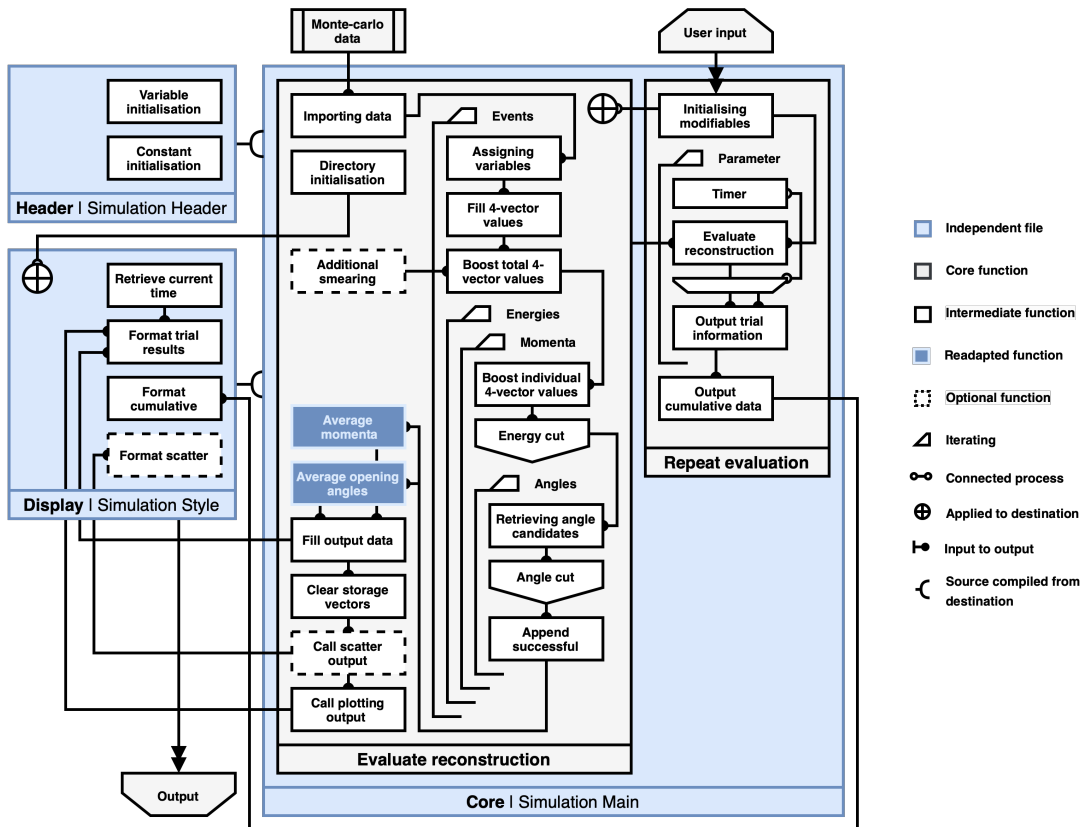


Figure 5.1: An overview of the fundamental components of the *WW* kinematic reconstruction program.

Loading simulation data and finding expected four-momenta

The simulation data was generated via the Monte-Carlo method, providing the final energies and momenta of the forward protons. This data was loaded and used to construct the expected WW four-momenta of the WW system. These values will vary depending on whether smearing was applied.

Constructing kinematic configurations of energy and four-momenta

Next, 1,000,000 kinematic configurations of the energy and momentum of the WW system were constructed in the CoM frame. These kinematic configurations include 1,000 energies within the limits of

$$E(WW) = [2M_W, 2(E(WW_{lab}) - M_W)] \quad (5.1)$$

and 1000 momenta of a single boson, in the z -direction, within the limits of

$$P_z(W) = \left[-\sqrt{\frac{(EWW)^2}{4 - (M_W)^2}}, \sqrt{\frac{(EWW)^2}{4 - (M_W)^2}} \right] \quad (5.2)$$

where M_W is the mass of the W boson from the data given and $E(WW_{lab})$ is the expected energy value of the WW system previously calculated.

Lorentz boost to the lab frame

The next step is to define the four-momenta of the W^+ and W^- bosons and boost these values parallel to the z -direction to the lab frame.

Performing an energy cut

The total energy of the W^+ and W^- bosons may now be compared for the reconstructed values to the expected WW energy, enabling the application of an energy cut, where energies larger than a lower limit were discarded. This energy limit is a modifiable parameter in our code.

Lepton decay angle

This information was then used to define the beta (β) and gamma (γ) terms unique to each of the reconstructed W bosons and calculate α , the lepton decay angle which is the angle between a W boson and the corresponding lepton they decay into.

Performing an angle cut

Next, an angle cut was performed on the reconstructed values that passed the energy cut. This was achieved by rotating our system in 1-degree increments about its azimuthal angle ϕ a set number of times. The number of times is a modifiable parameter to be optimised. For each of these degree increments, the lepton decay angle was found for that case and compared to the expected lepton decay angle. Candidates with a rotated lepton decay angle value outside the maximum range, another modifiable parameter we aimed to optimise, were discarded.

Averaging to determine final W directions

Subsequently, for all the reconstructed values which passed the cuts, the average momentum in the x , y and z directions was calculated. Further cuts were needed to ensure the averaged reconstructed W boson also passes the energy and angle cut. To achieve this, the energy of the averaged W boson was determined to enable another energy cut to be undertaken. If the averaged boson satisfied this energy cut, an angle cut was also completed. In the case of both energy and angle cut satisfaction, the averaged W boson was accepted. Otherwise, the boson farthest from the expected boson is discarded from the set of values, and averaging was redone until both cuts were satisfied.

Evaluating reconstruction efficiency

Finally, the success rate of each reconstruction was evaluated, and the angle difference between the reconstructed W boson directions and expected W boson directions was plotted. We expect a sharper peak at an angle difference of zero for more optimal parameters.

5.2 Reconstruction Overviews

5.2.1 Main Overview

The `run_simulation` function contains the reconstruction process. Several intermediate functions are referred to within it and are explained in subsequent sections. This explanation considers the optimised code without smearing or new averaging techniques. This allows for the investigation of modified mechanics and code structure. The smearing and averaging extensions were investigated with results in later sections.

The reconstruction process considers four inputs, which can either be defined directly through the terminal if running a single reconstruction process or a looping function. The reconstruction was adapted such that its information is provided from the external looping function. Here we identify the quantity of events we wish to reconstruct (`event_count`), the maximum limit for the energy cut (`max_wwe_diff`), the maximum limit for the angle cut (`angle_limit`), and the range of ϕ values to iterate over (`max_phi`).

The code creates a number of possibilities to be iterated over within a given range of energy and momenta. This provides us with 1,000,000 possibilities (considering 1,000 energies and momenta) filtered through an energy cut. The remaining candidates provided possibilities for their ϕ values, which were then cut again based on the defined criteria. Only candidates that survive the two filtering processes were kept and appended to storing vectors. The W boson momentum and opening angles were averaged, and the final values were directed to the styling functions and plotted.

```
1 string run_simulation(const int event_count, float max_wwe_diff, float
2   angle_limit, const int max_phi) {
3
4   // Creating main ROOT directory
5   TFile * f = TFile::Open("/Users/Username/Simulation/
6     Simulation_Output.root", "RECREATE");
```

```
5     TTree * t = new TTree("w1w2","W1W2");
6
7     int success_event_count = 0;
8     int non_success_event_count = 0;
9     successRate = 0;
10
11    load_data();
12    create_directory(t);
13
14    for(int event = 0; event < event_count; event++){
15
16        reference_variables(event);
17        fill_lab_values();
18        ww_boost_to_com();
19
20        for( int i = 0; i < wwe_range; i++ ){
21
22            for( int j = 0; j < wwp_range; j++ ){
23
24                wwe_com = w_mass*2 + i*2*(wwe_lab-w_mass)/(wwe_range-1);
25                wwp_com = -sqrt(wwe_com*wwe_com/4 - w_mass*w_mass) + 2*j
26                    *sqrt(wwe_com*wwe_com/4 - w_mass*w_mass)/(wwp_range
27                        -1);
28                w1w2_boost_to_lab();
29                wwe_diff = abs(w1e_lab + w2e_lab - wwe_lab);
30
31                if(wwe_diff < max_wwe_diff){ // Energy cut
32
33                    for( int k = 0; k < max_phi; k++ ){
34
35                        phi_increment = 2*TMath::Pi()*(k+1)/max_phi -
36                            TMath::Pi();
37                        get_angle_candidates(phi_increment);
38
39                        if( (abs(l1w1_angle_lab_candidate -
40                            l1w1_angle_lab) <= angle_limit)&&(abs(
41                            l2w2_angle_lab_candidate - l2w2_angle_lab) <=
42                                angle_limit) ){ // Angle cut
43
44                            append_values();
45
46                        } // Angle cut
47                    } // k
48                } // Energy cut
49            } // j
50        } // i
51
52        average_momenta();
53        average_opening_angles();
54
55        // Counting number of successful candidates
56        if(number_of_candidates == 0){
57            non_success_event_count += 1;
58        }
59        else{
60            success_event_count += 1;
61            t->Fill();
62        }
63    }
64}
```

```
57     cout << "Event " << event + 1 << " complete. Number of
58         candidates: " << number_of_candidates << endl;
59
60     clear_vectors();
61
62 } // Events
63
64 t->Write();
65
66 // Success rate of the reconstruction
67 successRate = ( (float)success_event_count / (float)event_count ) *
68     100. ;
69 cout << "***" << endl;
70 cout << "Reconstruction success: " << successRate << "%" << endl;
71 cout << "***" << endl;
72
73 // Cumulative data for repeated event plots
74 successRate_out.push_back( successRate );
75 daw1_all_out.push_back( std::accumulate(daw1_all.begin(), daw1_all.
76     end(), 0.0) / daw1_all.size() );
77 daw2_all_out.push_back( std::accumulate(daw2_all.begin(), daw2_all.
78     end(), 0.0) / daw2_all.size() );
79 daw1_all.clear();
80 daw2_all.clear();
81
82 // Plotting height defined suitably
83 max_events = event_count/8;
84 string print_location = format_plots(max_events);
85
86 return print_location;
87 } // run_simulation(event_count, max_wwe_diff, angle_limit, max_phi)
```

5.2.2 Repeated reconstruction overview

The automatic repeated evaluation of reconstructions subject to incremental parameter changes was handled by the function `loop_simulation`. The default constant parameters were initialised. A designated parameter was inserted to be modified at the location of "`selected parameter`" and equated to the variable `parameter`. This was subject to an incremental change, as explained in later sections.

Reconstruction was timed at each step, and the final results were recorded into a text file. Therefore, the global effects of the parameter could be measured, and the evolution of specific properties in terms of the increments plotted via a function within the styling.

```
1 int loop_simulation(float parameter_start, float parameter_end, int
2     parameter_count){
3
4     // Default
5     const int event_count = 500;
6     float max_wwe_diff = 10;
7     float angle_limit = 0.001;
8     int max_phi = 360;
```

```
8     for( int i = 0; i < parameter_count; i++ ){
9
10         float parameter_increase = (parameter_end-parameter_start)/
11             parameter_count;
12         float parameter = parameter_start + i*parameter_increase;
13
14         "selected parameter" = parameter;
15
16         auto start = std::chrono::high_resolution_clock::now();
17         print_location = run_simulation(event_count,max_wwe_diff,
18             angle_limit,max_phi);
19         auto end = std::chrono::high_resolution_clock::now();
20         auto duration = std::chrono::duration_cast<std::chrono::
21             milliseconds>(end - start);
22
23         ofstream plotfile(print_location+"plot_info.txt");
24
25         plotfile << "Plot information for file: " << print_location << "
26             \n\n";
27
28         plotfile << "--- Trial information ---\n";
29         plotfile << "Trial number: " << i+1 << " out of " <<
30             parameter_count << "\n";
31         plotfile << "Elapsed time: " << duration.count() << " ms" << "\n"
32             ";
33         plotfile << "Parameter value: " << parameter << "\n";
34         plotfile << "Success rate: " << successRate << "%\n\n";
35
36         plotfile << "--- Parameter initialisation ---\n";
37         plotfile << "Number of simulated events: " << event_count << "\n"
38             ";
39         plotfile << "Energy difference upper cut limit: " <<
40             max_wwe_diff << "\n";
41         plotfile << "Angle cut limit: " << angle_limit << "\n";
42         plotfile << "Azimuthal angle range: " << max_phi << "\n";
43
44         repeats.push_back(parameter);
45         time_out.push_back(duration.count());
46
47     }
48
49     format_plots_averages(print_location,repeats,daw1_all_out,
50         daw2_all_out,successRate_out,time_out);
51
52     cout << "***" << endl;
53     cout << " Task complete " << endl;
54     cout << "***" << endl;
55
56     return 0;
57 } //loop_simulation(parameter_start,parameter_end,parameter_count)
```

5.3 Function Overview

First, the header file, containing initialised variables, and the styling file were added into the program.

```
1 #include "/Users/Username/Simulation/Simulation_Header.h"
2 #include "/Users/Username/Simulation/Simulation_Style.c"
```

The three-dimensional carrier array previously explained, is used to take in the simulated particle data in the lab frame. The proton and lepton four-momenta data are assumed to be collected and used to reconstruct the W boson directions. The W boson information extracted at this point was used to verify the accuracy of the reconstruction process.

5.3.1 Loading Data Function

This function imported the simulation data from a text file. The energies (E), momentum in x , y and z direction (P_x , P_y , P_z) and masses (M) were extracted according to a particle identification number (PID), conventionally defined by the particle data group (PDG) [40] and their Monte-Carlo numbering scheme [41]. This was repeated along each line within the file for the select amount of simulation events, up to a maximum of 1,000 events, the amount of data available to the text file. Particle identifications that are not of interest to the reconstruction were skipped over by inserting them into unused variables: $c1, c2, c3, c4, c5, c6, c7$. The relevant particle identifications selected through the sequence of conditional statements include:

PID	Particle	Label
+2212	Proton 1	p_1
+2212	Proton 2	p_2
+24	W Boson 1 (+)	W^+
-24	W Boson 2 (-)	W^-
+13	Lepton 1 (Muon +)	$\bar{\ell}$
-13	Lepton 2 (Muon -)	ℓ

Table 5.1: Particle Identification and labels.

A negative value in front of the PID indicates the anti-particle of the associated identification. A PID value of 13 refers to a muon, but the reconstruction process itself should apply to a generalised lepton. Finally, the file is closed after importing all of the relevant information, and the stored data will be re-extracted in a later function.

```
1 int load_data(){
2     std::ifstream infile;
3     infile.open("/Users/joebacchus/Desktop/Full_Program/Simulation_Data.
4         txt");
5     std::string line;
6     for(int i = 0; i < event_count; i++){
7         std::getline(infile, line);
8         for(int j = 0; j < 10; j++) {
```

```
8     std::getline(infile, line);
9     std::istringstream iss(line);
10    iss >> pid >> c1 >> c2 >> c3 >> c4 >> c5 >> px >> py >> pz
11    >> energy >> mass >> c6 >> c7;
12    if(j==1&&pid==2212){particle_lab[0][0][i] = px; particle_lab
13    [0][1][i] = py; particle_lab[0][2][i] = pz; particle_lab
14    [0][3][i] = energy;}
15    if(j==2&&pid==2212){particle_lab[1][0][i] = px; particle_lab
16    [1][1][i] = py; particle_lab[1][2][i] = pz; particle_lab
17    [1][3][i] = energy;}
18    if(pid==24){particle_lab[2][0][i] = px; particle_lab[2][1][i]
19    ] = py; particle_lab[2][2][i] = pz; particle_lab[2][3][i]
20    = energy;}
21    if(pid== -24){particle_lab[3][0][i] = px; particle_lab[3][1][i]
22    ] = py; particle_lab[3][2][i] = pz; particle_lab[3][3][i]
23    = energy;}
24    if(pid==13){particle_lab[4][0][i] = px; particle_lab[4][1][i]
25    ] = py; particle_lab[4][2][i] = pz; particle_lab[4][3][i]
26    = energy;}
27    if(pid== -13){particle_lab[5][0][i] = px; particle_lab[5][1][i]
28    ] = py; particle_lab[5][2][i] = pz; particle_lab[5][3][i]
29    = energy;}
30    } //j
31    std::getline(infile, line);
32    } //i
33    infile.close();
34
35    return 0;
36 } //load_data()
```

5.3.2 Create Directory Function

To output the results that will be reconstructed, a directory was initialised to connect selected data to a plotting format defined within the styling file. Branches within the ROOT file were created and filled according to their reference (defined via the `&` before the variable in C++). Using a filling command applied towards the final stages of the reconstruction function, the designated information was directed to the ROOT file in preparation for the creation of the final plots in PDF format.

```
1 int create_directory(TTree * t){
2     // Decay opening angle of W +
3     t->Branch("daw1", &daw1);
4     // Decay opening angle of W -
5     t->Branch("daw2", &daw2);
6     // X-Momentum of W +
7     t->Branch("w1px_candidate", &wp_candidate[0]);
8     // Y-Momentum of W +
9     t->Branch("w1py_candidate", &wp_candidate[1]);
10    // Z-Momentum of W +
11    t->Branch("w1pz_candidate", &wp_candidate[2]);
12    // X-Momentum of W -
13    t->Branch("w2px_candidate", &wp_candidate[3]);
```

```
15 // Y-Momentum of W -
16 t->Branch("w2py_candidate", &wp_candidate[4]);
17 // Z-Momentum of W -
18 t->Branch("w2pz_candidate", &wp_candidate[5]);
19
20 return 0;
21 } //create_directory()
```

Each branch represents a property of the W bosons: the lepton decay opening angles with respect to each W^+ and W^- , as well as the momenta of the W^+ and W^- in cartesian x , y , and z directions.

5.3.3 Reference Variables Function

Although seemingly contradictory to the method of condensing variables into multi-dimensional arrays, unpacking values chosen for each event reconstruction before iterating through the conditions allowed for a repeated recollection of specific values prior to iterating over a number of events. This also avoided relocating array elements repeatedly within the loop and instead located a single variable.

```
1 int reference_variables(int event){
2
3     p1px_lab_event = particle_lab[0][0][event]; p1py_lab_event =
4         particle_lab[0][1][event]; p1pz_lab_event = particle_lab[0][2][
5             event]; p1e_lab_event = particle_lab[0][3][event];
6     p2px_lab_event = particle_lab[1][0][event]; p2py_lab_event =
7         particle_lab[1][1][event]; p2pz_lab_event = particle_lab[1][2][
8             event]; p2e_lab_event = particle_lab[1][3][event];
9     w1px_lab_event = particle_lab[2][0][event]; w1py_lab_event =
10        particle_lab[2][1][event]; w1pz_lab_event = particle_lab[2][2][
11            event]; w1e_lab_event = particle_lab[2][3][event];
12     w2px_lab_event = particle_lab[3][0][event]; w2py_lab_event =
13        particle_lab[3][1][event]; w2pz_lab_event = particle_lab[3][2][
14            event]; w2e_lab_event = particle_lab[3][3][event];
15     l1px_lab_event = particle_lab[4][0][event]; l1py_lab_event =
16        particle_lab[4][1][event]; l1pz_lab_event = particle_lab[4][2][
17            event]; l1e_lab_event = particle_lab[4][3][event];
18     l2px_lab_event = particle_lab[5][0][event]; l2py_lab_event =
19        particle_lab[5][1][event]; l2pz_lab_event = particle_lab[5][2][
20            event]; l2e_lab_event = particle_lab[5][3][event];
21
22     return 0;
23 } //reference_variables(event)
```

More specifically, the lab frame momentum (P_x , P_y , P_z) and energy E for each particle (the two p 's, ℓ , $\bar{\ell}$, W^+ , and W^-) in a given event were assigned to a variable such that each component of the momenta was referenced as a single unique variable.

5.3.4 Fill Lab Variables Function

The pre-built ROOT four-vectors were used to manipulate the particle data via Lorentz transformations. In this way, the relevant four-vectors were defined to perform the reconstruction and the W boson data for checking results.

```
1 int fill_lab_values(){
2
3     // Accuracy verification
4     w1_lab_ref.SetCoordinates(w1px_lab_event, w1py_lab_event,
5         w1pz_lab_event, w1e_lab_event);
6     w2_lab_ref.SetCoordinates(w2px_lab_event, w2py_lab_event,
7         w2pz_lab_event, w2e_lab_event);
8     w1_unit_distance_lab_ref = w1_lab_ref.Vect().Unit();
9     w2_unit_distance_lab_ref = w2_lab_ref.Vect().Unit();
10
11    // Reconstruction
12    p1_lab.SetCoordinates(p1px_lab_event, p1py_lab_event, p1pz_lab_event
13        , p1e_lab_event);
14    p2_lab.SetCoordinates(p2px_lab_event, p2py_lab_event, p2pz_lab_event
15        , p2e_lab_event);
16    l1_lab.SetCoordinates(l1px_lab_event, l1py_lab_event, l1pz_lab_event
17        , l1e_lab_event);
18    l2_lab.SetCoordinates(l2px_lab_event, l2py_lab_event, l2pz_lab_event
        , l2e_lab_event);
19    l1_unit_distance_lab = l1_lab.Vect().Unit();
20    l2_unit_distance_lab = l2_lab.Vect().Unit();
21
22    return 0;
23 } //fill_lab_values()
```

The resulting four-momenta were provided in the following form for each particle:

$$P_\mu = \begin{pmatrix} P_x \\ P_y \\ P_z \\ E \end{pmatrix} \quad (5.3)$$

The unit vector directions of these defined four-momenta for the leptons and bosons were also defined to evaluate the opening angle calculations in later parts of the code.

5.3.5 WW Boost to Centre-of-Mass Frame Function

Reconstructing the momenta and energy of the WW boson vertex was also a source of interest, since this information allows the construction of the Lorentz boost necessary to take the individual W boson particles to their CoM frame. The ROOT pre-built boosting mechanism was defined to be applied strictly along the z -direction, which can then be applied to the lab frame four-momenta.

The values for the protons' four-momenta were used to determine the sum of the energy and momenta from the WW system.

```

1 int ww_boost_to_com(){
2
3     // Reconstruction
4     wwpz_lab = p1pz_lab_event + p2pz_lab_event;
5     if(wwpz_lab<=0.0){direction_parameter = -1;}
6     else{direction_parameter = 1;}
7     wwe_lab = invariant_mass - (p1e_lab_event + p2e_lab_event);
8
9     ww_com.SetCoordinates(-(p1px_lab_event+p2px_lab_event), -(p1py_lab_event+p2py_lab_event), -wwpz_lab, wwe_lab);
10    wz_boost.SetBeta(-direction_parameter*ww_com.Beta());
11
12    return 0;
13 } // ww_boost_to_com()

```

The transformation is calculated by considering energy conservation. The proton energies may be obtained in terms of the final proton energies and the original W boson energies:

$$E(p_1) + E(p_2) = E(p'_1) + E(p'_2) + E(W^+) + E(W^-) \quad (5.4)$$

and the invariant mass (or CoM energy given as E_{CoM}) of the system is calculated as follows:

$$E(p_1) + E(p_2) = E_{CoM} = 13\text{TeV} \quad (5.5)$$

Manipulating this result yields:

$$E(W^+) + E(W^-) = 13\text{TeV} - [E(p'_1) + E(p'_2)] \quad (5.6)$$

where the final proton energy is from the preloaded data. This provides us with the energy of the WW system in the lab frame.

Next, applying conservation of momentum gives:

$$P(p'_1) = -[P(W^+) + P(W^-)] \quad (5.7)$$

where we can define a direction parameter (d), which takes values according to:

$$d = \begin{cases} -1, & \text{if } P(p'_1) + P(p'_2) < 0 \\ 1, & \text{if } P(p'_1) + P(p'_2) > 0 \end{cases} \quad (5.8)$$

The final WW four-vector in the lab frame is therefore given as:

$$P_\mu^{WW} \begin{pmatrix} -(P_x(p'_1) + P_x(p'_2)) \\ -(P_y(p'_1) + P_y(p'_2)) \\ -(P_z(p'_1) + P_z(p'_2)) \\ E(W^+) + E(W^-) \end{pmatrix} \quad (5.9)$$

This was then implemented in the code. Furthermore, within this function, we also define β used in Lorentz transformations, which is used in the next function to boost the reconstructed W bosons from their CoM frame to the lab frame.

5.3.6 W_1W_2 Boost to lab Frame Function

This function uses the reconstruction values (the 1,000,000 kinematic configurations of momentum and energy of the WW system) to determine the momentum and energy of a single boson. The bosons were assumed to be "mirror images" of each other, meaning their momenta are of opposite signs but the same magnitudes.

With this assumption, the energy of one W boson was set as half the energy of the total WW system. The z -direction of a single boson's momentum was the chosen reconstructed value for that kinematic configuration, leaving the x and y momenta to be determined. The remaining momenta will be determined in terms of the azimuthal angle ϕ . This was done such that an angle cut may later be applied, as it allows variation of x -momentum and y -momentum according to this angle value.

```
1 int w1w2_boost_to_lab(){
2
3     // Reconstruction
4     w1p_selected = sqrt(wwe_com*wwe_com/4-w_mass*w_mass - wwp_com*
5         wwp_com);
6     w1px_com_selected = w1p_selected*cos(w1phi_com_selected);
7     w1py_com_selected = w1p_selected*sin(w1phi_com_selected);
8     w1_com.SetCoordinates( w1px_com_selected,   w1py_com_selected,
9         wwp_com, wwe_com/2);
10    w2_com.SetCoordinates(-w1px_com_selected, -w1py_com_selected, -
11        wwp_com, wwe_com/2);
```

The magnitude of the momentum in the $x-y$ direction can be determined from the energy in the CoM frame (E_{CoM}), the mass of the W boson (M_W), and the momentum of one W boson in the z -direction (P_z):

$$|P_{xy}| = \sqrt{\frac{(E_{CoM})^2}{4 - (M_W)^2} - (P_z)^2} \quad (5.10)$$

The momenta in the x and y directions can now be defined as:

$$P_x = |P_{xy}|\cos(\phi) \quad (5.11)$$

$$P_y = |P_{xy}|\sin(\phi) \quad (5.12)$$

where ϕ is set to 0 for W_1 and $-\pi$ for W_2 for simplicity.

Using the momenta components defined so far, the W_1 boson four-momenta in the WW CoM frame is given by:

$$P_{W1} = (P_x, P_y, P_z, \frac{E_{CoM}}{2}) \quad (5.13)$$

Due to symmetry, the W_2 boson simply has the same four-momenta in the opposite direction:

$$P_{W2} = (-P_x, -P_y, -P_z, \frac{E_{CoM}}{2}) \quad (5.14)$$

```

1   w1_lab = wz_boost(w1_com);
2   w2_lab = wz_boost(w2_com);
3   w1e_lab = w1_lab.E(); w1px_lab = w1_lab.Px(); w1py_lab = w1_lab.Py();
4   w1pz_lab = w1_lab.Pz();
5   w2e_lab = w2_lab.E(); w2px_lab = w2_lab.Px(); w2py_lab = w2_lab.Py()
6   ; w2pz_lab = w2_lab.Pz();
7   w1_beta = sqrt(w1px_lab*w1px_lab + w1py_lab*w1py_lab + w1pz_lab*
8   w1pz_lab)/w1e_lab;
9   w2_beta = sqrt(w2px_lab*w2px_lab + w2py_lab*w2py_lab + w2pz_lab*
10  w2pz_lab)/w2e_lab;
11  w1_gamma = 1/sqrt(1-w1_beta*w1_beta);
12  w2_gamma = 1/sqrt(1-w2_beta*w2_beta);
13  l1w1_angle_lab = acos( 1/w1_beta - w1_gamma * w_mass*(1/w1_beta -
14  w1_beta)/2/l1e_lab_event );
15  l2w2_angle_lab = acos( 1/w2_beta - w2_gamma * w_mass*(1/w2_beta -
16  w2_beta)/2/l2e_lab_event );
17
18  return 0;
19 } // w1w2_boost_to_com()
```

The four-momenta for W_1 and W_2 were then boosted from the WW CoM frame to the lab frame using the β value calculated from the simulation data. To apply this mechanism effectively, ROOT enables the application of a boosting function to four-momenta in the same method as applying a function. The boosting function in this case was defined previously within the `ww_boost_to_com()` function. For each boson, new values of β_W and γ_W were determined for the W_1 and W_2 rest frame:

$$\beta_W = \frac{|P_W|}{E_W} \left(= \frac{v}{c} \right) \quad (5.15)$$

$$\gamma_W = \frac{1}{\sqrt{1 - \beta^2}} \quad (5.16)$$

This is used to determine the lepton decay angle between each boson and the corresponding lepton:

$$\alpha = \cos^{-1} \left[\frac{1}{\beta_W} - \gamma_W \frac{M_W}{2E_l} \left(\frac{1}{\beta_W} - \beta_W \right) \right] \quad (5.17)$$

where E_l is the lepton energy obtained from the provided data.

5.3.7 Get Angle Candidates Function

We now rotate our boosted W bosons and calculate α at each orientation of ϕ . This was achieved by increasing our ϕ value in defined increments, determining our new four-momenta in this situation and finally calculating the lepton decay angle for each of these new orientations.

```

1 int get_angle_candidates(float phi_increment){
2
3     // Reconstruction
4     w1phi_lab = w1_lab.Phi();
5     w1pxy_lab = sqrt(w1px_lab*w1px_lab + w1py_lab*w1py_lab);
6     w1_lab_candidate.SetCoordinates(w1pxy_lab*cos(w1phi_lab+
7         phi_increment), w1pxy_lab*sin(w1phi_lab+phi_increment), w1pz_lab,
8         w1e_lab);
9     w1_unit_distance_lab = w1_lab_candidate.Vect().Unit();
10    l1w1_angle_lab_candidate = acos(l1_unit_distance_lab.Dot(
11        w1_unit_distance_lab));
12
13    w2phi_lab = w2_lab.Phi();
14    w2pxy_lab = sqrt(w2px_lab*w2px_lab + w2py_lab*w2py_lab);
15    w2_lab_candidate.SetCoordinates(w2pxy_lab*cos(w2phi_lab+
16        phi_increment), w2pxy_lab*sin(w2phi_lab+phi_increment), w2pz_lab,
17        w2e_lab);
18    w2_unit_distance_lab = w2_lab_candidate.Vect().Unit();
19    l2w2_angle_lab_candidate = acos(l2_unit_distance_lab.Dot(
20        w2_unit_distance_lab));
21
22    return 0;
23 //get_angle_candidates(phi_increment)

```

First, the four-momentum of a single reconstructed W was redefined in the following form:

$$\begin{pmatrix} |P_{xy}| \cos(\phi + \phi_k) \\ |P_{xy}| \sin(\phi + \phi_k) \\ P_z \\ E \end{pmatrix} \quad (5.18)$$

where P_{xy} was calculated from the now boosted x and y components of the W bosons' momenta, given as:

$$|P_{xy}| = \sqrt{(P_x)^2 + (P_y)^2} \quad (5.19)$$

The rotated W boson four-momentum was then used to compute the unit vectors \hat{W} of the W boson candidates.

Next, the angle between each lepton candidate and its corresponding W boson candidate was obtained in the laboratory frame by taking the dot product of the lepton unit

vector, \hat{l} , in the laboratory frame (using the text file) with the corresponding W boson unit vector in the lab frame, calculated below:

$$\alpha = \arccos(\hat{W} \cdot \hat{l}) \quad (5.20)$$

This angle was computed for the other W boson and anti-lepton candidates.

5.3.8 Append Values Function

Within this function, all the four-momenta of the W bosons which survive were saved and used later to calculate the average of the momenta of these candidates.

In addition to this, the function also determined the dot product between a surviving W boson direction (\vec{W}_2) and the W boson from the simulated data's direction (\vec{W}_1). Calculating this gives the cosine of the angle difference between the two bosons ($\cos(W_{12})$).

$$\cos(W_{12}) = \frac{\vec{W}_1 \cdot \vec{W}_2}{|\vec{W}_1| |\vec{W}_2|} \quad (5.21)$$

This was calculated for plotting comparisons later.

```
1 int append_values() {
2
3     vector_w1phi_lab_candidate.push_back(w1_lab_candidate.Phi());
4     vector_w2phi_lab_candidate.push_back(w2_lab_candidate.Phi());
5
6     vector_wp_lab_candidate[0].push_back(w1_lab_candidate.Px());
7     vector_wp_lab_candidate[1].push_back(w1_lab_candidate.Py());
8     vector_wp_lab_candidate[2].push_back(w1_lab_candidate.Pz());
9
10    vector_wp_lab_candidate[3].push_back(w2_lab_candidate.Px());
11    vector_wp_lab_candidate[4].push_back(w2_lab_candidate.Py());
12    vector_wp_lab_candidate[5].push_back(w2_lab_candidate.Pz());
13    vector_w1w1.push_backacos(w1_unit_distance_lab.Dot(
14        w1_unit_distance_lab_ref));
15    vector_w2w2.push_backacos(w2_unit_distance_lab.Dot(
16        w2_unit_distance_lab_ref));
17
18    return 0;
19 } //append_values()
```

5.3.9 Average Momenta Function

The total number of W boson candidates (n) which pass both the energy and angle cut was defined. An average was taken for the momentum of these candidates in all three directions, with the average of each direction given in the form:

$$P_{av} = \frac{P_1 + P_2 + \dots + P_n}{n} \quad (5.22)$$

```
1 int average_momenta(){
2
3     number_of_candidates = vector_w1phi_lab_candidate.size();
4
5     for(int j = 0; j < 6; j++){
6         wp_candidate[j] = 0;
7         for(int i = 0; i < number_of_candidates; i++){wp_candidate[j] +=
8             vector_wp_lab_candidate[j][i];}
9         wp_candidate[j] = wp_candidate[j]/static_cast<float>(
10            number_of_candidates);
11    }
12
13    return 0;
14 } //average_momenta()
```

5.3.10 Average Opening Angles Function

Using the values obtained for $\cos(W_{12})$, an average was found for each difference of the surviving boson and simulated data angle.

```
1 int average_opening_angles(){
2
3     if(number_of_candidates != 0){
4         daw1 = 0;
5         daw2 = 0;
6         for(int l = 0; l < number_of_candidates; l++){
7             daw1 = daw1 + vector_w1w1[l];
8             daw2 = daw2 + vector_w2w2[l];
9         }
10
11         daw1 = daw1/static_cast<float>(number_of_candidates);
12         daw2 = daw2/static_cast<float>(number_of_candidates);
13
14         daw1_all.push_back(daw1);
15         daw2_all.push_back(daw2);
16     }
17
18     return 0;
19 } //average_opening_angles()
```

5.3.11 Clear Vectors Function

After an event was completed, vectors storing values for ϕ and angles between the reconstructed boson and the expected boson directions were cleared. This is so that we can use the same vectors for the following events.

```
1 int clear_vectors(){
2
3     vector_w1phi_lab_candidate.clear();
4     vector_w2phi_lab_candidate.clear();
5
6     for(int k = 0; k < 6; k++){vector_wp_lab_candidate[k].clear();}
```

```
7     vector_w1w1.clear();
8     vector_w2w2.clear();
9
10    return 0;
11 } // clear_vectors()
```

5.3.12 Proton Smearing

Due to various sources of uncertainty within this reconstruction process, the physical quantities measured undergo distortion, referred to as smearing. The inclusion of this increment is unavoidable due to experimental limitations. Smearing can arise from a multitude of sources, including the precision of the detector and other external elements.

Specifically in forward tagging, as protons collide in the LHC, they can interact with atomic nuclei or other particles in the beam and subsequently divert from their original path, thereby altering the physical measurements of the momentum and energy of the protons and creating uncertainties in the reconstructed data. This effect is known as proton smearing and was investigated in further sections.

Without accounting for smearing in the code for the simulation, the reconstructed data will not accurately represent the characteristics of the particles. The lack of smearing translates onto the plots as strong peaks and a broadened distribution, making it more difficult to identify differences within the plots. This distortion of the distribution could deform the Gaussian, negatively impacting the analysis of the uncertainties. Including smearing in the code would eradicate a standard bias that causes the data to deviate from more accurate values systematically.

```
1 int add_smearing(float smearing_extent){
2
3     float sigma_p1e = 2.5 + ((0.5*invariant_mass-p1e_lab_event)/
4         p1e_lab_event) * 50;
5     float sigma_p2e = 2.5 + ((0.5*invariant_mass-p2e_lab_event)/
6         p2e_lab_event) * 50;
7
8     sigma_p1e = p1e_lab_event + smearing_extent * gRandom->Gaus(0.0,
9                     sigma_p1e);
10    sigma_p2e = p2e_lab_event + smearing_extent * gRandom->Gaus(0.0,
11                     sigma_p2e);
12
13    wwe_lab = invariant_mass - sigma_p1e - sigma_p2e;
14    p1_lab.SetCoordinates(p1px_lab_event, p1py_lab_event, p1pz_lab_event
15                          , sigma_p1e);
16    p2_lab.SetCoordinates(p2px_lab_event, p2py_lab_event, p2pz_lab_event
17                          , sigma_p2e);
18
19    return 0;
20 }
```

Gaussian smearing was used on the protons to create some “uncertainty” on the final protons’ measured energy and momentum, as measurements taken from the detector may not be entirely accurate. The Gaussian was defined as follows:

$$\sigma(\zeta) = 2.5 + 50\zeta \quad (5.23)$$

where ζ_1 , the rate of change of energy loss of the first proton after the collision, is defined as follows:

$$\zeta_1 = \frac{0.5E_{CoM} - E(p'_1)}{E(p'_1)} \quad (5.24)$$

and mirrored for the second proton as ζ_2 .

The Gaussian is therefore in the form of $f(0, \sigma)$ where the mean is 0 and the standard deviation is σ .

Using this, the energy of the protons ($E_{\sigma p'_1}$) can be redefined as:

$$E_{\sigma p'_1} = E_{p'_1} + R[f(0, \sigma)] \quad (5.25)$$

where $R[f(0, \sigma)]$ is a random value selected from the defined Gaussian distribution.

From the smeared values, the energy of the WW system can be finally redefined as:

$$E_{WW} = E_{CoM} - [E_{p'_{\sigma 1}} + E_{p'_{\sigma 2}}] \quad (5.26)$$

5.3.13 Average Filter function

To better reconstruct the most optimal solution, the following averaging function was introduced to replace the previous methods of `average_opening_angles` and `average_momenta` simultaneously. However, the latter function was still kept and implemented internally within the new function more cautiously. To do so, a Boolean condition was initialised negatively and only validated once a certain criterion has been satisfied: the averaged reconstructed event independently satisfies the cuts. A preliminary check was applied to verify whether any candidates survived the initial selection process that was enforced by the previous functions. In the case that no candidates survive, the loop is broken out immediately, and the averaging mechanism is ignored so that no solution is provided.

The average four-momentum P_μ^W , was then constructed for all surviving candidates for the individual W bosons defined using Eq. 5.27 and 5.28.

```

1 int average_filter(float max_wwe_diff, float angle_limit){
2     bool pass_cut = false;
3     float w1e_candidate_av;
4     float w2e_candidate_av;
5
6     number_of_candidates = vector_w1phi_lab_candidate.size();
7
8     while(pass_cut == false){

```

```

9
10     if (number_of_candidates == 0) {
11         pass_cut = true;
12         break;
13     }
14
15     average_momenta();
16     w1e_candidate_av = sqrt(w_mass*w_mass + wp_candidate[0]*
17                             wp_candidate[0] + wp_candidate[1]*wp_candidate[1] +
18                             wp_candidate[2]*wp_candidate[2]);
19     w2e_candidate_av = sqrt(w_mass*w_mass + wp_candidate[3]*
18                             wp_candidate[3] + wp_candidate[4]*wp_candidate[4] +
19                             wp_candidate[5]*wp_candidate[5]);
w1_lab_average.SetCoordinates(wp_candidate[0], wp_candidate[1],
                             wp_candidate[2], w1e_candidate_av);
w2_lab_average.SetCoordinates(wp_candidate[3], wp_candidate[4],
                             wp_candidate[5], w2e_candidate_av);

```

The energy of the averaged momenta ($P_{x(av)}$, $P_{y(av)}$, $P_{z(av)}$) for the W boson:

$$E_{av} = \sqrt{M_W^2 + P_{x(av)}^2 + P_{y(av)}^2 + P_{z(av)}^2} \quad (5.27)$$

and the averaged four-momenta of our W bosons:

$$P_\mu^W = \begin{pmatrix} P_{x(av)} \\ P_{y(av)} \\ P_{z(av)} \\ E_{av} \end{pmatrix} \quad (5.28)$$

P_μ^W was then passed through the original selection process since the average may lie outside of the selection criteria, and so the average solution must also be compatible with this. If the criteria are satisfied, the Boolean variable is set to `true` and the while loop terminates. If this new averaging mechanism is provided with a non-zero amount of candidates, then at least one reconstructed solution will be guaranteed. This is due to the fact that the candidates independently satisfy both cuts, and so in the case that the candidates are filtered until there is a single possibility remaining, it has already been verified to be a solution.

```

1     if (abs(w1e_candidate_av + w2e_candidate_av - wwe_lab) <
2         max_wwe_diff){
3         l1w1_angle_lab = 0;
4         l2w2_angle_lab = 0;
5         w1e_lab = w1_lab_average.E(); w1px_lab = w1_lab_average.Px()
6             ; w1py_lab = w1_lab_average.Py(); w1pz_lab =
7                 w1_lab_average.Pz();
8         w2e_lab = w2_lab_average.E(); w2px_lab = w2_lab_average.Px()
9             ; w2py_lab = w2_lab_average.Py(); w2pz_lab =
10                w2_lab_average.Pz();
11         w1_beta = sqrt(w1px_lab*w1px_lab + w1py_lab*w1py_lab +
12                         w1pz_lab*w1pz_lab)/w1e_lab;
13         w2_beta = sqrt(w2px_lab*w2px_lab + w2py_lab*w2py_lab +
14                         w2pz_lab*w2pz_lab)/w2e_lab;
15         w1_gamma = 1/sqrt(1-w1_beta*w1_beta);

```

```
9     w2_gamma = 1/sqrt(1-w2_beta*w2_beta);
10    l1w1_angle_lab = acos( 1/w1_beta - w1_gamma * w_mass*(1/
11        w1_beta - w1_beta)/2/l1e_lab_event );
12    l2w2_angle_lab = acos( 1/w2_beta - w2_gamma * w_mass*(1/
13        w2_beta - w2_beta)/2/l2e_lab_event );
14    l1w1_angle_lab_candidate = acos(l1_unit_distance_lab.Dot(
15        w1_lab_average.Vect().Unit()));
16    l2w2_angle_lab_candidate = acos(l2_unit_distance_lab.Dot(
17        w2_lab_average.Vect().Unit()));
18
19    if( (abs(l1w1_angle_lab_candidate - l1w1_angle_lab) <=
19        angle_limit)&&(abs(l2w2_angle_lab_candidate -
19        l2w2_angle_lab) <= angle_limit) ){
20        pass_cut = true;
21    }//if
22
23 }//if
```

For average solutions that do not pass the selection process, the individual W boson unit vectors for each candidate in the lab frame, \hat{W}_1 and \hat{W}_2 , were defined and their dot product was taken with the respective average W boson unit vectors, $\hat{\bar{W}}_1$ and $\hat{\bar{W}}_2$:

$$\cos(\theta_1) = \hat{W}_1 \cdot \hat{\bar{W}}_1 \quad (5.29)$$

$$\cos(\theta_2) = \hat{W}_2 \cdot \hat{\bar{W}}_2 \quad (5.30)$$

where θ_1 and θ_2 are the angular separations between the individual candidate and the average candidate's direction for each boson respectively. This was repeated for each candidate until the candidate farthest from the average is determined. This candidate was then removed from the average and the new average passes through the selection process again. Candidates were repeatedly removed until a new average survives the selection process, in which case the Boolean variable becomes `true` and the while loop terminates. This yields an average direction which coincides with the selection criteria and is therefore a valid solution for the WW boson directions.

```
1     if (pass_cut == false){
2         float w1a_magnitude;
3         float w2a_magnitude;
4         float maximum_mag_value_angle = 0;
5         float maximum_mag = 0;
6         for (int c = 0; c < number_of_candidates; c++){
7
8             w1_angle_diff.SetCoordinates(vector_wp_lab_candidate[0] [
8                 c],vector_wp_lab_candidate[1][c],
8                 vector_wp_lab_candidate[2][c]);
9             w2_angle_diff.SetCoordinates(vector_wp_lab_candidate[3] [
9                 c],vector_wp_lab_candidate[4][c],
9                 vector_wp_lab_candidate[5][c]);
10            w1a_magnitude = (w1_angle_diff.Unit()).Dot(
10                w1_lab_average.Vect().Unit());
11            w2a_magnitude = (w2_angle_diff.Unit()).Dot(
11                w2_lab_average.Vect().Unit());
```

```

12
13         if (w1a_magnitude + w2a_magnitude >
14             maximum_mag_value_angle){
15             maximum_mag_value_angle = w1a_magnitude +
16                 w2a_magnitude;
17             maximum_mag = c;
18         }
19
20         for (int i = 0; i < 6; i++){
21             vector_wp_lab_candidate[i].erase(vector_wp_lab_candidate[i].
22                 begin() + maximum_mag);
23         }
24         vector_w1w1.erase(vector_w1w1.begin() + maximum_mag);
25         vector_w2w2.erase(vector_w2w2.begin() + maximum_mag);
26         number_of_candidates -= 1;
27     }
28     return 0;
}

```

To better appreciate the structure of this newly implemented logic, a simplified illustration is provided below. In this setting, we consider the input to take in the successful reconstructed candidates. We then apply the conditional loop until either we have no reconstructions or the averaged solution satisfies both cuts. This is then outputted directly to be plotted.

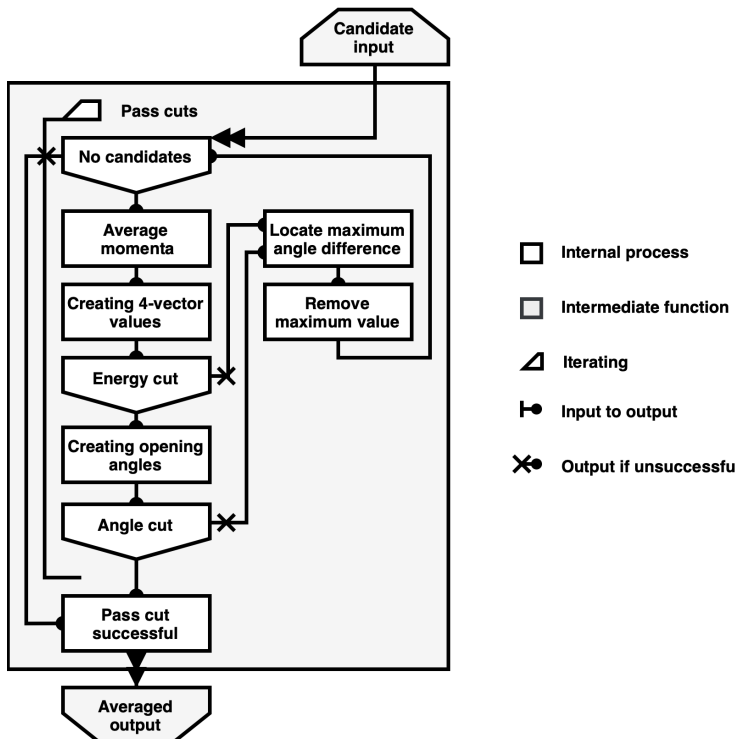


Figure 5.2: Re-adapted averaging mechanism overview.

Results & Analysis

6.1 Preliminary Findings

The provided simulation was initialised with a number of modifiable parameters. This includes:

- Number of energy reconstruction values
- Number of momentum reconstruction values
- Number of different azimuthal angle orientations.
- The energy limit.
- The angle limit.

Firstly, the optimal parameter values were investigated, with the aim of achieving the highest reconstruction success rate and lowest deviation of the reconstructed W boson directions from the true directions. Minimisation of code run-time was a secondary aim, and was prioritised where results were not significantly impacted.

The number of reconstructed energy and momenta values was not investigated due to the self-imposed restriction of 1,000,000 reconstructed WW system events. This avoids generating unnecessary candidates, which is exponentially more computationally expensive. Thus, both are defined as constants (set to 1,000) in the header file.

To provide a benchmark for comparison, parameters will be optimised relative to initial results. These are defined in the original code by Prof. M. Campanelli and Y. He, which implemented a simple averaging mechanism. The three parameters were initially configured as:

Parameter	Energy Limit	Angle Limit	Azimuthal increments
Value	10 (GeV)	0.001 (rad)	360 (Iterations)

Table 6.1: Initial parameters of the original code.

These parameters provided results with a high success rate but large deviations between reconstructed events and targets. Under these restrictions, W boson pairs were reconstructed for 470 out of 500 events, resulting in a 94% success rate. The mean of the reconstructed W_1 angle differences was 0.1777 rad, and the standard deviation was 0.2054

rad. The W_2 angle differences resulted in a mean of 0.1786 rad and a standard deviation of 0.2076 rad. Visually, the angle difference plots shown in Fig. 6.1 suffer from prolonged tails. This provides the aim of ensuring the mean of the differences and the standard deviation is minimised as close to zero as possible.

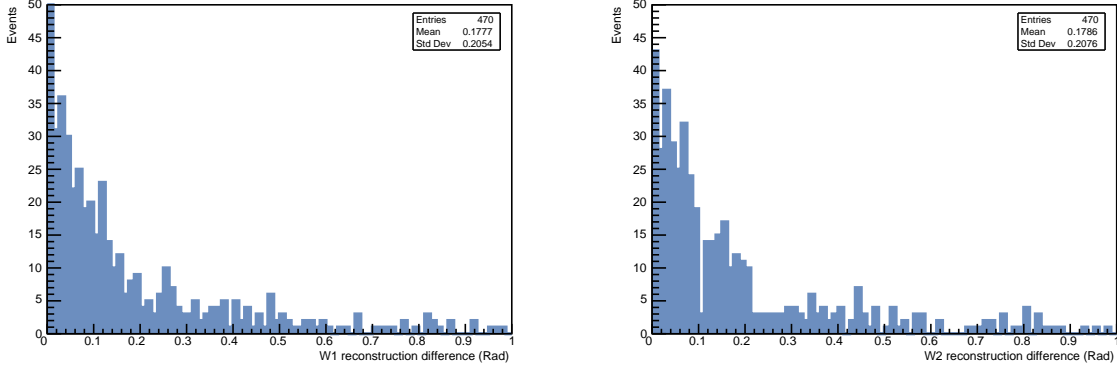


Figure 6.1: Original angle reconstruction differences with 500 events.

Results may also be produced for the momenta reconstructions of both W bosons. Though not as representative of the accuracy of reconstructed directions, they reveal some of the physics behind the kinematic events and confirm the simulation is functioning as expected.

In the plots shown in Fig. 6.2, there is apparent symmetry between the momenta along the x and y directions for both bosons. This reflects the absence of a net momentum within the $x - y$ plane. On the other hand, the z -momentum displays less coherent behaviour as this momentum corresponds to the boosted direction.

We will first discuss the effects of tuning the three parameters of interest across incremental values. For each one, we generated reconstructed directions for 500 events over 20 incremental values. These were selected to range from much before the initial chosen value to much after. These ranges are summarised in the table below:

Parameter	Energy Limit	Angle Limit	Azimuthal increments
Initial value	1 (GeV)	0.0001 (Rad)	180 (Iterations)
Final value	20 (GeV)	0.002 (Rad)	720 (Iterations)
Increment	0.95 (GeV)	0.00005 (Rad)	27 (Iterations)

Table 6.2: Incremental changes in parameters being optimised.

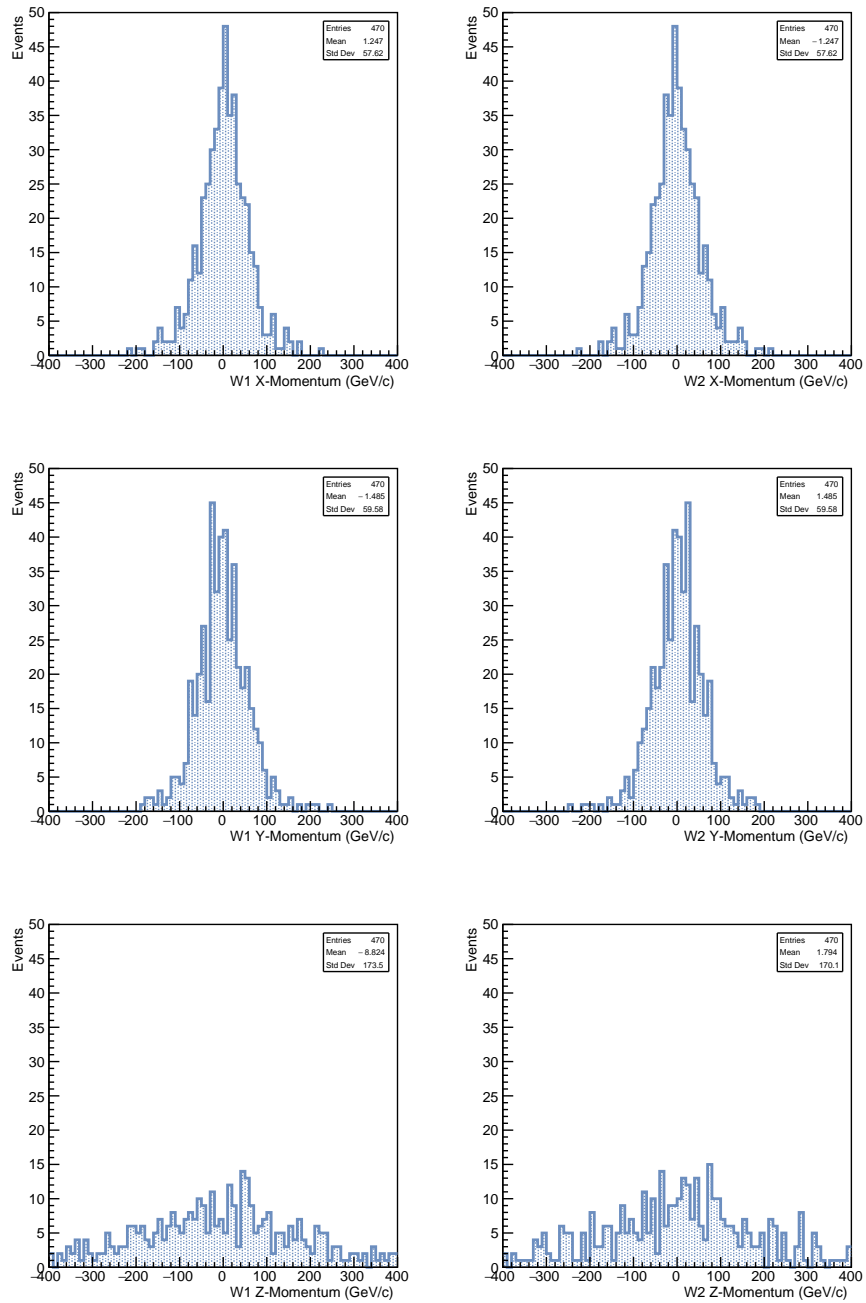


Figure 6.2: Original momenta reconstruction with 500 events.

We will now present our results for each parameter we aimed to optimise.

6.1.1 Energy limit

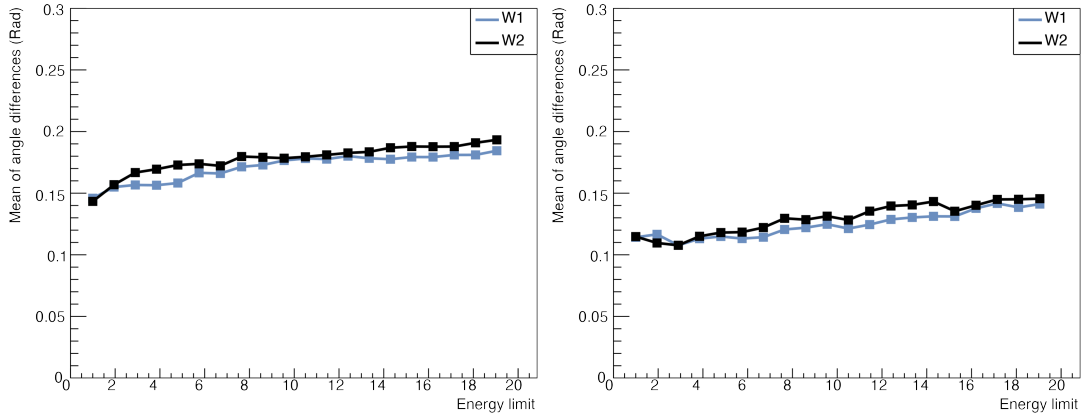
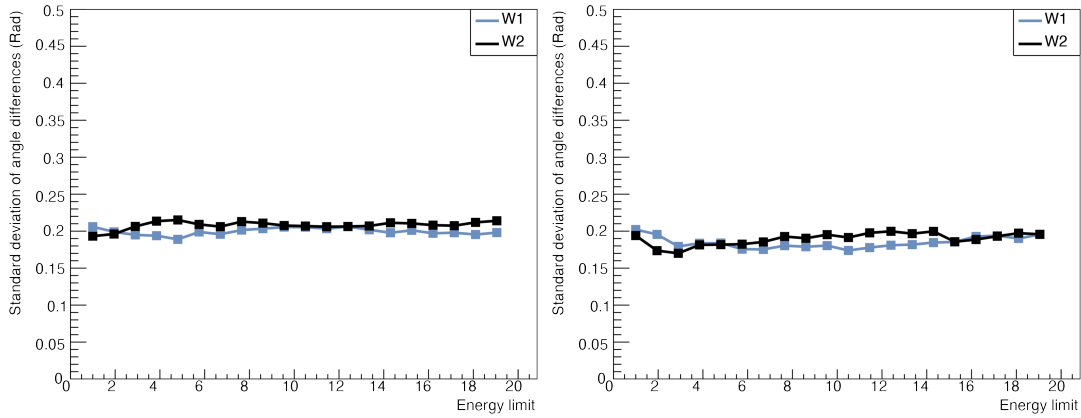


Figure 6.3: Mean of reconstructed W boson direction differences for increasing energy limits with original averaging (left) and re-adapted averaging (right).



	Original averaging		Re-adapted averaging	
	W1-Boson	W2-Boson	W1-Boson	W2-Boson
Maximum std. dev.	0.2061	0.2151	0.2022	0.1998
Energy limit	12.4	4.8	1	12.4
Minimum std. dev.	0.1889	0.1933	0.1739	0.1701
Energy limit	4.8	1	10.5	2.9

Figure 6.4: Standard deviation of reconstructed W boson direction differences for increasing energy limits with original averaging (left) and re-adapted averaging (right).

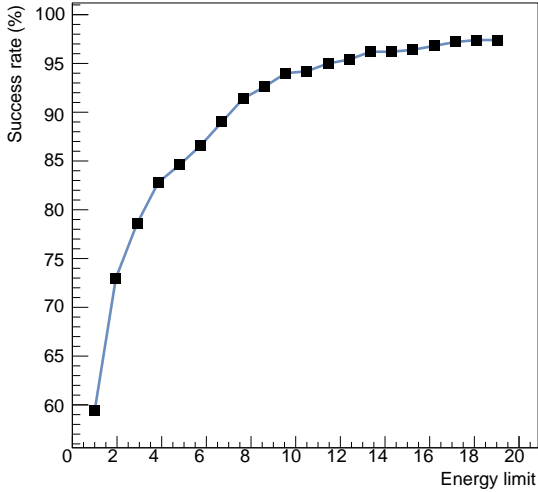


Figure 6.5: Success rate of reconstructed W boson direction differences for increasing energy limits.

As seen in Fig. 6.3, as the energy cut for the selection process increases, there is also a slight increase in the mean deviation between the truth and reconstructed W direction for both bosons. This result aligns with the physical expectation since a greater limit for the energy cut allows more candidates to survive these selection criteria. This leads to a greater variety of possible reconstruction configurations contributing to the reconstructed W direction. Therefore, the average deviation between this and the true direction will likely be negatively impacted. This suggests that a smaller energy cut should be applied to decrease the deviation. However, Fig. 6.5 implies that a small energy cut equally produced a worsened reconstruction rate. The slight trough in the mean deviation for both bosons encourages the use of 6.7 GeV as an optimal parameter. This allows for a high reconstruction rate of 89% but also ensures that these constructions are of greater accuracy.

Fig. 6.5 shows that at an energy cut of approximately 9 GeV, the rate of success approaches a maximum and starts to level out to 97.4%. This implies that beyond this point, the energy cut is too large as almost all the reconstructed W bosons were allowed through rather than filtered.

The new averaging mechanism presents a drastic difference in the deviations between the truth-level and reconstructed directions in both the mean and the standard deviation. The minimum mean deviation using the original averaging mechanism is approximately equal to the maximum mean deviation with the new mechanism implemented. The standard deviation with this new mechanism is also significantly lower than the original. This suggests that this approach has a more significant impact on the accuracy of the WW direction reconstruction than the variation of individual parameters.

6.1.2 Angle limit

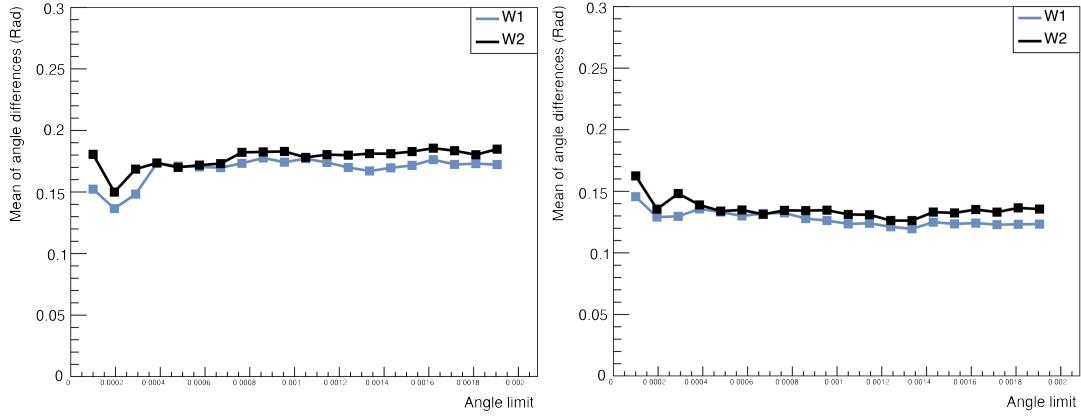


Figure 6.6: Mean of reconstructed W boson direction differences for increasing angle limits with original averaging (left) and re-adapted averaging (right).

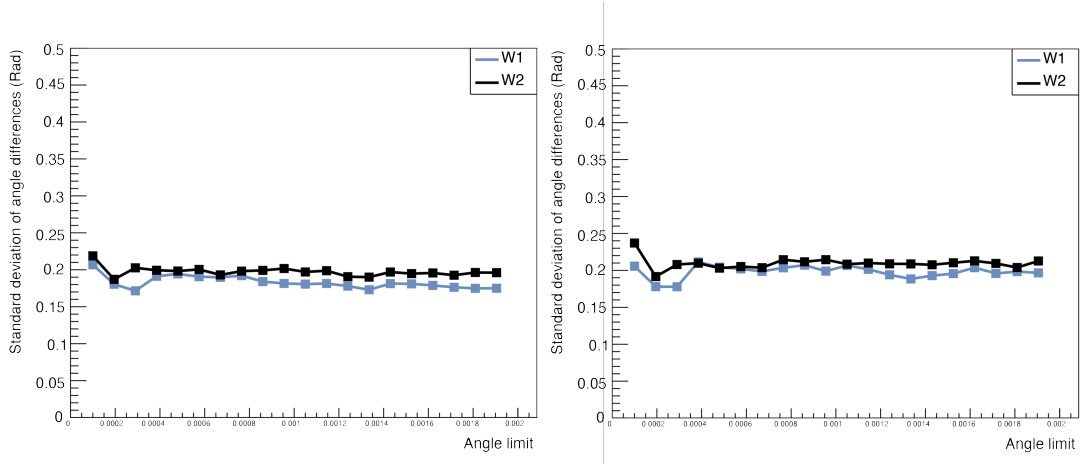


Figure 6.7: Standard deviation of reconstructed W boson direction differences for increasing angle limits with original averaging (left) and re-adapted averaging (right).

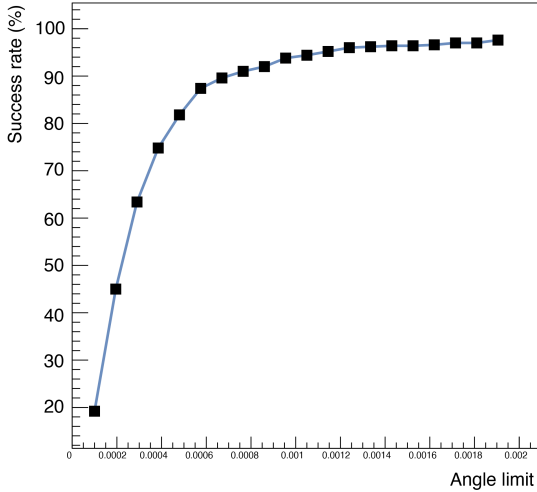


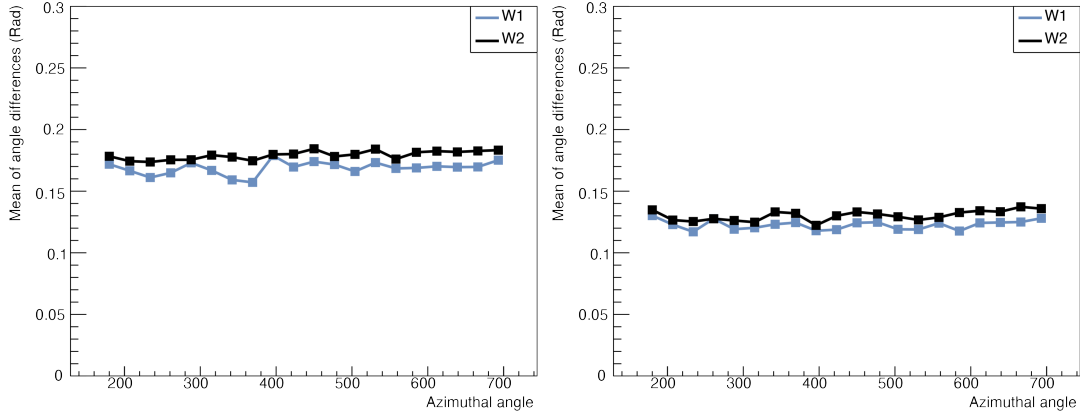
Figure 6.8: Success rate of reconstructed W boson direction differences for increasing angle limits.

As seen in Fig. 6.6 and 6.7, as the angle cut for the selection process increases, the mean deviation and spread of those deviations between the truth and reconstructed W direction for both bosons remain fairly constant. The only discrepancy is a clear dip at an angle of 0.000195 rad but is followed by a low reconstruction rate of 45%, which is too small to allow for this to be our optimal value. The slight trough observed in the mean and standard deviation therefore encourages the use of 0.00048 rad as an optimal parameter with a reasonable reconstruction rate of 81.8%.

Results shown in Fig 6.8 indicate that increasing the cut leads to a higher reconstruction rate, but opting for a lower cut can impose tighter constraints on the deviation. This is observed as success rate levels off to about 95% at 0.001145 rad, implying that beyond this angle limit, the constraints will no longer achieve optimal results.

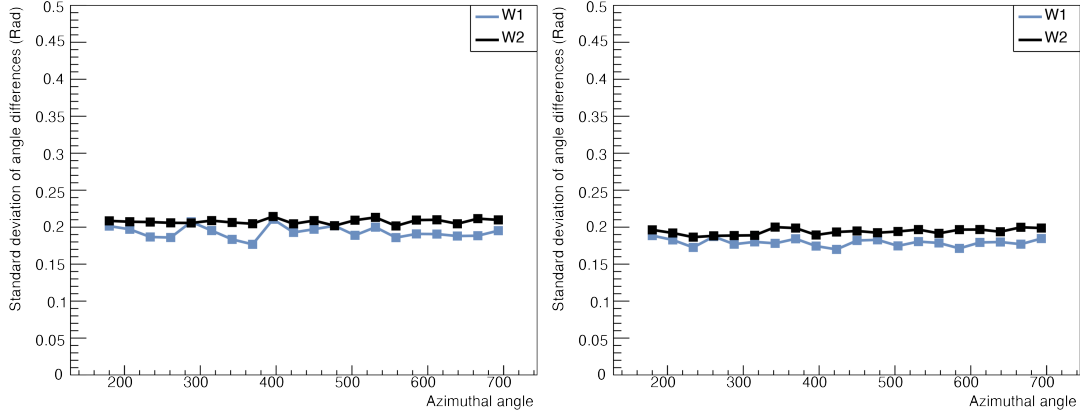
After implementing the new averaging mechanism, there is a considerable improvement in the deviations between the truth level and reconstructed directions, as with the energy cut. The mean and standard deviation show a large difference compared to the previous mechanism. To illustrate, the minimum mean deviation achieved by the old mechanism was roughly equivalent to the maximum mean deviation obtained with the new approach. Furthermore, the standard deviation with the new mechanism was notably lower than the original. These findings suggest that this new approach has a more significant effect on enhancing the accuracy of the WW direction reconstruction beyond variations in individual parameters.

6.1.3 Azimuthal increments



	Original averaging		Re-adapted averaging	
	W1-Boson	W2-Boson	W1-Boson	W2-Boson
Maximum mean	0.1789	0.1844	0.1302	0.1373
Azimuthal inc.	396	450	180	666
Minimum mean	0.1572	0.1737	0.1170	0.1223
Azimuthal inc.	369	234	234	396

Figure 6.9: Mean of reconstructed W boson direction differences for increasing azimuthal increments with original averaging (left) and re-adapted averaging (right).



	Original averaging		Re-adapted averaging	
	W1-Boson	W2-Boson	W1-Boson	W2-Boson
Maximum std. dev.	0.2107	0.2144	0.1886	0.2001
Azimuthal inc.	396	396	180	342
Minimum std. dev.	0.1768	0.2020	0.1699	0.1894
Azimuthal inc.	369	477	423	396

Figure 6.10: Standard deviation of reconstructed W boson direction differences for increasing azimuthal increments with original averaging (left) and re-adapted averaging (right).

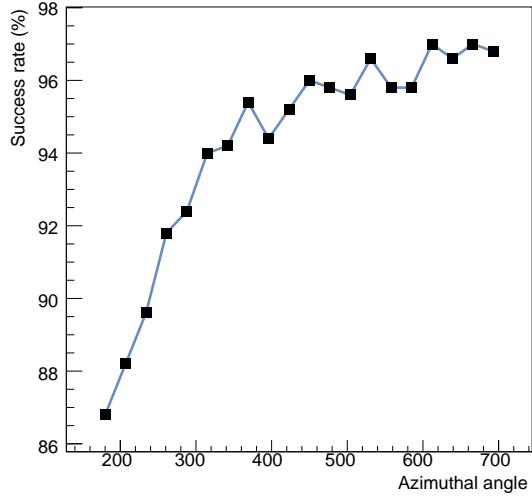


Figure 6.11: Success rate of reconstructed W boson direction differences for increasing azimuthal increments.

As noted in Fig. 6.9 and 6.10, as the azimuthal increments increase, the mean and standard deviation remain fairly constant, with mean values of the original averaging remaining between 0.1572 rad and 0.1789 rad for W_1 . This pattern is also seen in the standard deviation plots, remaining nearly constant for W_2 . At the observed maximum and minimum values, the success rate is relatively high, with 95.4% at 369 increments and 94.4% at 396 increments, showing great efficiency at most points.

Focusing on the success rate alone, results shown in Fig. 6.11 are jagged, this is likely due to the range of success rate being within 88% and 98%, allowing the plot to show dips and peaks with greater resolution. Notably, as the azimuthal angle increments increase, the success rate generally increases. There are observed peaks near multiples of 180 increments (i.e. 360, 480, 540 and 720), implying that the computations may miss boson values that dip after a maximum point. This leads to the optimal value selected as 558 increments, which gives a reasonable success rate of 95.8%.

Considering the new averaging mechanism, the mean angle difference between the reconstructed and true boson decreased by an average of 0.4 rad, an improvement compared to the original averaging method. The mean and standard deviation are almost constant, showing the small effect the azimuthal angle increments have on the mean value deduced.

6.1.4 Optimised results

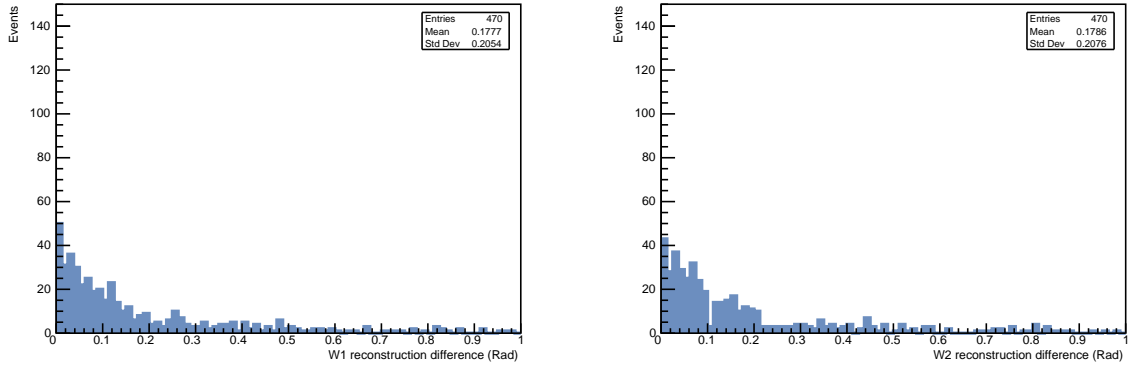
For all investigated parameters, values can simply be increased to obtain improved reconstruction rates. This is due to the 'brute-force' nature of the approach, as limitations are defined so they place restrictions on the amount of generated candidates satisfying the set conditions. We can approach the optimisation more generally from two perspectives: one in which we aim to maximise this amount, sacrificing reconstruction accuracy, a property determined by the mean and standard deviation of the angle differences. Alternatively, the parameters may be minimised as much as possible with the aim of obtaining more accurate reconstructed directions, but with the risk of reducing the chances of producing such events significantly.

Having discussed the individual effects of these parameters on the reconstruction accuracy and success rate, it is important to consider that in combination, the most competitive value may not necessarily provide the best results. Nevertheless, they offer us a good estimate of the combined optimal parameters and an insight into their roles. In this way, we can now discern the outcomes of our reconstruction differences subject to their most optimised settings.

Fig. 6.12 shows renormalised (modified axes to better facilitate comprehension) plots of the differences between the two reconstructed W boson directions and the true values, subject to the initial parameter settings and standard averaging mechanism. The results implementing the deduced optimal parameters are presented in Fig. 6.13, and demonstrate much sharper peaks for a discrepancy of zero radians. However, as mentioned above, for the increased parameter values (energy and angle limits), there is a loss in success rate, as we restrict ourselves to a smaller range of possibilities to pass the cuts. For this reason, our W_1 and W_2 success rate for the optimised parameters was reduced from 94% to 81.2%. The optimisation, in this case, is thus chosen to partially sacrifice the event reconstruction rate in order to ensure that the results are as accurate as possible (improving by just over 1% for each). Similar reductions are observed across the standard deviations. Therefore, there is only so much amelioration that can be done to improve the accuracy of the reconstructions with only parameter modifications (without significantly impacting the event success rate).

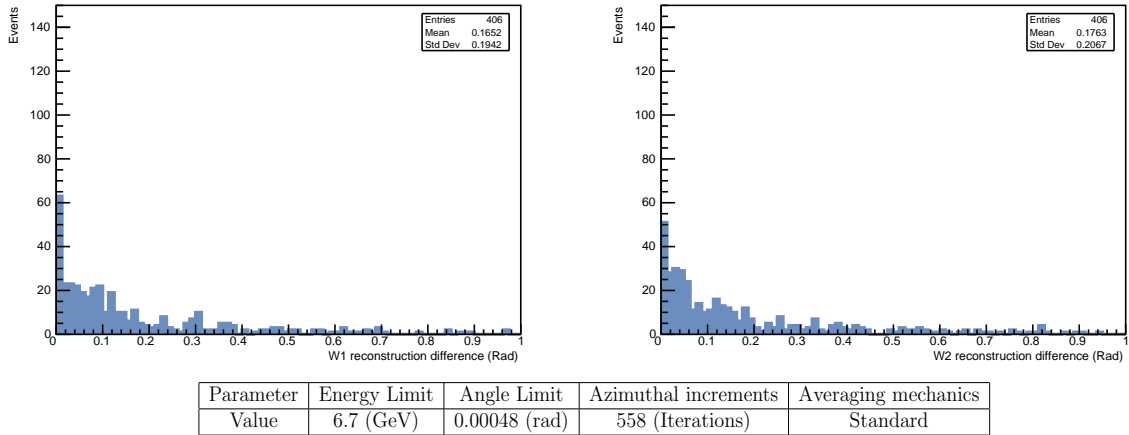
To attain better accuracies, adaptations of the code mechanisms were implemented. Having implemented a re-adapted averaging function, the most optimal parameters were again determined using the same iterative method as before. Results from this new mechanism, shown in Fig. 6.14, clearly present sharper solutions towards the mean of zero. There is also a reduction in the clustering of events within particular locations, equally benefiting the mean of these angle differences. Numerically, we obtain for the W_1 reconstruction a difference of the means that is 46% closer to nought than the initial parameters with the standard averaging function and 34% closer for W_2 . Likewise, the standard deviations for these differences are 19% lower for the W_1 case and 6% lower for W_2 than the initial reconstructions. As well as drastically improving the accuracy of the reconstructed events, unlike the standard averaging function, the new mechanism ceases to affect the success rate negatively, resulting in a 96.8% reconstruction rate for the latter results.

CHAPTER 6. RESULTS & ANALYSIS



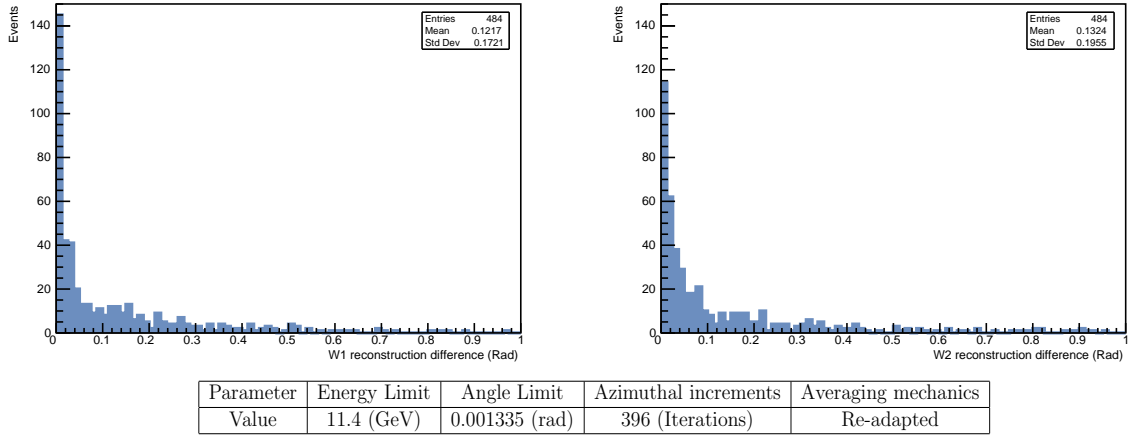
Parameter	Energy Limit	Angle Limit	Azimuthal increments	Averaging mechanics
Value	10 (GeV)	0.001 (rad)	360 (Iterations)	Standard

Figure 6.12: Reconstructed directions using initial parameters and the standard averaging mechanism.



Parameter	Energy Limit	Angle Limit	Azimuthal increments	Averaging mechanics
Value	6.7 (GeV)	0.00048 (rad)	558 (Iterations)	Standard

Figure 6.13: Reconstructed directions using initial parameters and the standard averaging mechanism.



Parameter	Energy Limit	Angle Limit	Azimuthal increments	Averaging mechanics
Value	11.4 (GeV)	0.001335 (rad)	396 (Iterations)	Re-adapted

Figure 6.14: Reconstructed directions using optimised parameters and the re-adapted averaging mechanism.

6.1.5 Implementing smearing

In a more physically feasible situation, one must consider the uncertainty and imperfections in measurement that come about from a practical experiment. To simulate this, we apply smearing to the process of determining the expected energy of the WW system. This was investigated using the best reconstruction results, those that used the optimised parameters with re-adapted averaging. These results are shown in Fig. 6.15. Overlaying the smearing plots in red over the un-smeared results filled in blue, we notice that the peak is reduced, accuracy is slightly reduced, and the success rate falls. Despite this, the plots follow similar trends to the pre-smearing case, and even offer better accuracies than the un-smeared initial results.

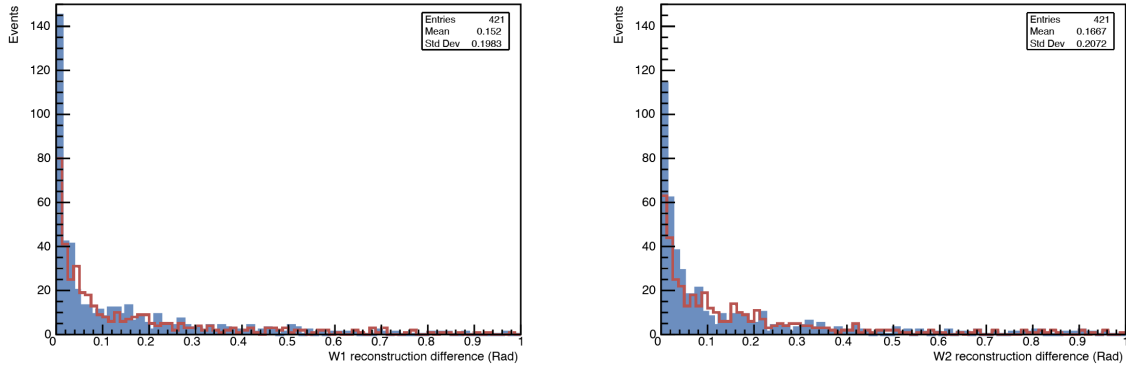


Figure 6.15: Reconstructed directions using optimised parameters and the re-adapted averaging mechanism considering proton smearing.

Conclusion

7.1 Summary of Results

The WW directions from the $WW \rightarrow \ell\bar{\nu}\ell\nu$ decay were successfully simulated and reconstructed using the optimised code. Code redundancies were removed, multi-variable reduction employed, and carrier arrays introduced, resulting in a run-time performance improvement of 26% over the original code, using initial parameters proposed by M. Campanelli and Y. He.

The impact of the azimuthal resolution, lepton decay angle cut and WW system energy cut was investigated. The initial optimised energy limit of 6.7 GeV, an angle limit of 0.0048 rad and 558 azimuthal increments provided more W bosons being reconstructed at smaller deviations between the true and reconstructed directions. Comparing with baseline parameters of an energy limit of 10 GeV, angle limit of 0.001 rad and 360 azimuthal orientations, the optimised values showed a sharper peak at smaller angle differences and a more subdued tail, resulting in a 1% average decrease in the mean angle deviation and measured standard deviation compared to the baseline. This implies there are more candidates which align with the expected W boson direction, suggesting the parameter optimisation was somewhat successful.

A new averaging system was implemented to verify that the averaged W boson solutions satisfy the initial selection criteria. If the criteria were not met, the candidate furthest from the average is removed and this new average is then fed back into the selection process until at least one reconstructed solution survives, which will always be a valid candidate for the W boson direction.

Optimised parameters were also found for the re-adapted averaging, these parameters being an energy limit of 11.4 GeV, an angle limit of 0.001335 rad and 396 azimuthal orientations. When compared to the baseline, there is an observed peak at 0 rad which is approximately 3 times bigger when using the re-adapted averaging, indicating a significantly greater number of candidates aligning with the expected W boson direction. There is also a large reduction in mean and standard deviation for this re-adapted averaging when compared to both the baseline and the optimised original averaging, showing our achieved results are consistent. The calculated means for W_1 reconstruction were 46% closer to zero than the initial parameters using the original averaging function, while for W_2 , the difference was 34% closer. Furthermore, the standard deviations for these differences were 19% lower for W_1 and 6% lower for W_2 compared to the initial reconstructions. The new mechanism not only greatly improves the accuracy of reconstructed events, but

it also does not negatively affect the success rate, resulting in a reconstruction rate of 96.8% for the latter results, unlike the standard averaging function.

7.2 Further Improvements

There are several ways to further develop and refine the reconstruction technique. For instance, although parallel looping using *OpenMP* proved inefficient, it can occasionally offer significant boosts for specific computational looping tasks. It may be necessary to utilise synchronisation mechanisms, such as locks, semaphores, or barriers, to regulate and allocate access to shared resources among threads. Additionally, static analysis and dynamic testing tools may be employed to detect potential concurrency-related errors before they occur.

As we have already considered the effects of proton smearing on the reconstructed events, it would be of interest to further develop these experimental considerations by taking into account additional detector smearing on other particles. We could then also investigate whether the optimised parameters are unaffected by these smearing processes.

For the current reconstruction, W masses are taken to be constants of the same value for both negative and positive alternatives of the bosons. To refine our technique, we could instead consider taking the W mass as a distribution rather than a single value. In this way, although we would heavily multiply the computational cost of running such a simulation, the results would offer incredibly precise predicted reconstructions. This would ensure a wider range of solutions to our simulation, leading to a greater likeness with experimental data.

Alternative methods, inspired by recent improvements in machine learning methods, could equally provide us with more optimal approaches to reconstructing W directions. In particular, deep-learning techniques [8] may offer a new strategy for the reconstruction process. One might use the extensive data collected from Monte-Carlo simulators to train a model (e.g. regression) capable of refining the candidate selections. Furthermore, we could also implement more extensive regression analysis on the data obtained from iterating over specific parameters. In this way, one might deduce more detailed predictions of the parameter effects.

We would like to thank Prof. Mario Campanelli and Yi He for the provision of the initial kinematic reconstruction code and for the relevant technical advice throughout the project.

Bibliography

- [1] G. Arnison, A. Astbury, B. Aubert, *et al.*, “Experimental observation of isolated large transverse energy electrons with associated missing energy at s=540 GeV,” *Physics Letters B*, vol. 122, no. 1, pp. 103–116, 1983, ISSN: 0370-2693. DOI: [https://doi.org/10.1016/0370-2693\(83\)91177-2](https://doi.org/10.1016/0370-2693(83)91177-2). [Online]. Available: <https://www.sciencedirect.com/science/article/pii/0370269383911772>.
- [2] G. Arnison, A. Astbury, B. Aubert, *et al.*, “Experimental observation of lepton pairs of invariant mass around 95 GeV/c² at the CERN SPS collider,” *Physics Letters B*, vol. 126, no. 5, pp. 398–410, 1983, ISSN: 0370-2693. DOI: [https://doi.org/10.1016/0370-2693\(83\)90188-0](https://doi.org/10.1016/0370-2693(83)90188-0). [Online]. Available: <https://www.sciencedirect.com/science/article/pii/0370269383901880>.
- [3] M. Trzebinski, “Prospects for Proton-Proton Measurements with Tagged Protons in ATLAS,” *arXiv*, 2019. DOI: <https://doi.org/10.48550/arXiv.1909.10827>.
- [4] R Staszewski, “The AFP Project,” *arXiv*, 2011. DOI: <http://dx.doi.org/10.5506/APhysPolB.42.1615>.
- [5] C. Royon and N. Cartiglia, “The AFP and CT-PPS projects,” *arXiv*, 2015. DOI: <https://doi.org/10.48550/arXiv.1503.04632>.
- [6] V. Khachatryan, A. Sirunyan, A. Tumasyan, *et al.*, “Search for new resonances decaying via WZ to leptons in proton–proton collisions at s=8TeV,” *Physics Letters B*, vol. 740, pp. 83–104, 2015, ISSN: 0370-2693. DOI: <https://doi.org/10.1016/j.physletb.2014.11.026>. [Online]. Available: <https://www.sciencedirect.com/science/article/pii/S0370269314008284>.
- [7] A. Ballestrero, E. Maina, and G. Pelliccioli, “Polarized vector boson scattering in the fully leptonic WZ and ZZ channels at the LHC,” *Journal of High Energy Physics*, vol. 2019, no. 9, 2019. DOI: [10.1007/jhep09\(2019\)087](10.1007/jhep09(2019)087). [Online]. Available: <https://doi.org/10.1007Fjhep0928201929087>.
- [8] M. Grossi, J. Novak, B. Kerševan, and D. Rebuzzi, “Comparing traditional and deep-learning techniques of kinematic reconstruction for polarization discrimination in vector boson scattering,” *The European Physical Journal C*, vol. 80, no. 12, 2020. DOI: <10.1140/epjc/s10052-020-08713-1>. [Online]. Available: <https://doi.org/10.11402Fepjc2Fs10052-020-08713-1>.
- [9] A. Sirunyan, A. Tumasyan, W. Adam, *et al.*, “Search for anomalous couplings in boosted ww/wz→qq production in proton–proton collisions at s=8 tev,” *Physics Letters B*, vol. 772, pp. 21–42, 2017, ISSN: 0370-2693. DOI: <https://doi.org/10.1016/j.physletb.2017.06.009>. [Online]. Available: <https://www.sciencedirect.com/science/article/pii/S0370269317304690>.

BIBLIOGRAPHY

- [10] V. Abazov, B. Abbott, B. Acharya, *et al.*, “Limits on anomalous trilinear gauge boson couplings from WW, WZ and w production in pp-bar collisions at sqrt(s)=1.96 tev,” *Physics Letters B*, vol. 718, no. 2, pp. 451–459, 2012. DOI: 10.1016/j.physletb.2012.10.062. [Online]. Available: <https://doi.org/10.1016/j.physletb.2012.10.062>.
- [11] M. Bilenky, J.-L. Kneur, F. Renard, and D. Schildknecht, “The potential of a new linear collider for the measurement of the trilinear couplings among the electroweak vector bosons,” *Nuclear Physics B*, vol. 419, no. 2, pp. 240–253, 1994. DOI: 10.1016/0550-3213(94)90041-8. [Online]. Available: [https://doi.org/10.1016/0550-3213\(94\)90041-8](https://doi.org/10.1016/0550-3213(94)90041-8).
- [12] M. S. Chanowitz and M. Golden, “Like-charged gauge-boson pairs as a probe of electroweak symmetry breaking,” *Phys. Rev. Lett.*, vol. 61, pp. 1053–1056, 9 1988. DOI: 10.1103/PhysRevLett.61.1053. [Online]. Available: <https://link.aps.org/doi/10.1103/PhysRevLett.61.1053>.
- [13] J. Bagger, V. Barger, K. Cheung, *et al.*, “Cern lhc analysis of the strongly interacting ww system: Gold-plated modes,” *Phys. Rev. D*, vol. 52, pp. 3878–3889, 7 1995. DOI: 10.1103/PhysRevD.52.3878. [Online]. Available: <https://link.aps.org/doi/10.1103/PhysRevD.52.3878>.
- [14] C Csáki and P Tanedo, “Beyond the Standard Model,” en, *arXiv*, pp. 18–49, 2015. DOI: <https://doi.org/10.5170/cern-2015-004.169>. [Online]. Available: <http://cds.cern.ch/record/2119546>.
- [15] T. W. B. Kibble, “The Standard Model of Particle Physics,” 2014. DOI: 10.48550/ARXIV.1412.4094. [Online]. Available: <https://arxiv.org/abs/1412.4094>.
- [16] A. Salam and J. C. Ward, “Weak and electromagnetic interactions,” *Il Nuovo Cimento (1955-1965)*, vol. 11, pp. 568–577, 1959. DOI: https://doi.org/10.1142/9789812795915_0034.
- [17] G. Arnison, A. Astbury, B. Aubert, *et al.*, “Further evidence for charged intermediate vector bosons at the SPS collider,” *Physics Letters B*, vol. 129, no. 3, pp. 273–282, 1983, ISSN: 0370-2693. DOI: [https://doi.org/10.1016/0370-2693\(83\)90860-2](https://doi.org/10.1016/0370-2693(83)90860-2). [Online]. Available: <https://www.sciencedirect.com/science/article/pii/0370269383908602>.
- [18] J. Ellis, “Top, Higgs, Diboson and Electroweak Fit to the Standard Model Effective Field Theory,” *arXiv:2012.02779v3*, 2022. DOI: <https://doi.org/10.48550/arXiv.2012.02779>. [Online]. Available: <https://arxiv.org/abs/2012.02779>.
- [19] C. Collaboration†‡, T Aaltonen, S Amerio, *et al.*, “High-precision measurement of the W boson mass with the CDF II detector,” *Science*, vol. 376, no. 6589, pp. 170–176, 2022. DOI: <https://www.science.org/doi/10.1126/science.abk1781>.
- [20] A. Tumasyan, W. Adam, J. Andrejkovic, T. Bergauer, and S. Chatterjee, vol. 105, no. 7, 2022. DOI: 10.1103/physrevd.105.072008. [Online]. Available: <https://doi.org/10.1103/physrevd.105.072008>.
- [21] A. M. Sirunyan, A. Tumasyan, W. Adam, *et al.*, “ W^+W^- Boson pair production in proton-proton collisions at $\sqrt{s} = 13$ TeV,” *Phys. Rev. D*, vol. 102, p. 092001, 9 2020. DOI: 10.1103/PhysRevD.102.092001. [Online]. Available: <https://link.aps.org/doi/10.1103/PhysRevD.102.092001>.

BIBLIOGRAPHY

- [22] S. Roth, *Precision electroweak physics at electron-positron colliders*. Springer Berlin, 2014.
- [23] D. Weiskopf, M. Borchers, T. Ertl, *et al.*, “Explanatory and illustrative visualization of special and general relativity,” *IEEE Transactions on Visualization and Computer Graphics*, vol. 12, no. 4, pp. 522–534, 2006. DOI: [10.1109/TVCG.2006.69](https://doi.org/10.1109/TVCG.2006.69).
- [24] P. Martins, L. N. Alves, and J. C. Mendes, “On the dynamics of accelerated observers in special relativity,” in *2017 European Conference on Circuit Theory and Design (ECCTD)*, 2017. DOI: [10.1109/ECCTD.2017.8093266](https://doi.org/10.1109/ECCTD.2017.8093266).
- [25] G. Aad, J. Butterworth, J Thion, *et al.*, “The ATLAS experiment at the CERN Large Hadron Collider,” *Jinst*, vol. 3, S08003, 2008. DOI: <https://dx.doi.org/10.1088/1748-0221/3/08/S08003>.
- [26] J. W. G. Thomason, R. Garoby, S. Gilardoni, L. J. Jenner, and J. Pasternak, “Proton driver scenarios at cern and rutherford appleton laboratory,” *Phys. Rev. ST Accel. Beams*, vol. 16, p. 054801, 5 2013. DOI: [10.1103/PhysRevSTAB.16.054801](https://doi.org/10.1103/PhysRevSTAB.16.054801). [Online]. Available: <https://link.aps.org/doi/10.1103/PhysRevSTAB.16.054801>.
- [27] N. A. Ky and N. T. H. Van, “Was the Higgs boson discovered?” *arXiv preprint arXiv:1503.08630*, 2015.
- [28] O. Brüning, H. Burkhardt, and S. Myers, “The large hadron collider,” *Progress in Particle and Nuclear Physics*, vol. 67, no. 3, pp. 705–734, 2012, ISSN: 0146-6410. DOI: <https://doi.org/10.1016/j.ppnp.2012.03.001>. [Online]. Available: <https://www.sciencedirect.com/science/article/pii/S0146641012000695>.
- [29] L. Evans, “The Large Hadron Collider,” *New Journal of Physics*, vol. 9, no. 9, p. 335, 2007. DOI: [10.1088/1367-2630/9/9/335](https://doi.org/10.1088/1367-2630/9/9/335). [Online]. Available: <https://dx.doi.org/10.1088/1367-2630/9/9/335>.
- [30] F. Ledroit-Guillon, “ATLAS prospects for beyond the Standard Model searches,” *Nuclear Physics B - Proceedings Supplements*, vol. 200-202, pp. 7–16, 2010, The International Workshop on Beyond the Standard Model Physics and LHC Signatures (BSM-LHC), ISSN: 0920-5632. DOI: <https://doi.org/10.1016/j.nuclphysbps.2010.02.062>. [Online]. Available: <https://www.sciencedirect.com/science/article/pii/S0920563210000824>.
- [31] S. Murk, “Trigger algorithms and monte carlo event generation for dijet searches in atlas and beyond,” 2017.
- [32] N. Soni, “ATLAS Forward Detectors and Physics,” *arXiv*, 2010. DOI: <https://doi.org/10.48550/arXiv.1006.5426>.
- [33] L Adamczyk, R. Appleby, P Bank, *et al.*, “AFP: A proposal to install proton detectors at 220 m around ATLAS to complement the ATLAS high luminosity physics program,” *ATL-COM-LUM-2011-006*, 2011.
- [34] S. A. Khalek, B Allongue, F Anghinolfi, *et al.*, “The ALFA roman pot detectors of ATLAS,” *Journal of Instrumentation*, vol. 11, no. 11, P11013, 2016. DOI: <https://doi.org/10.48550/arXiv.1609.00249>.
- [35] J. Pinfold, “ATLAS and ultra high energy cosmic ray physics,” in *EPJ Web of Conferences*, EDP Sciences, vol. 145, 2017, p. 10 001.
- [36] R. Frühwirth, M. Regler, R. K. Bock, H. Grote, and D. Notz, “Data Analysis Techniques for High-Energy Physics,” 2000.

BIBLIOGRAPHY

- [37] Y. Langsam, M. J. Augenstein, and A. M. Tenenbaum, *Data Structures Using C and C++ (2nd Ed.)* USA: Prentice Hall Press, 1996, ISBN: 0130369977.
- [38] R. L. Kruse and A. J. Ryba, *Data Structures and Program Design in C++*. USA: Prentice-Hall, Inc., 1998, ISBN: 0137689950.
- [39] R. Chandra, L. Dagum, D. Kohr, R. Menon, D. Maydan, and J. McDonald, *Parallel programming in OpenMP*. Morgan kaufmann, 2001.
- [40] R. L. Workman *et al.*, “Review of Particle Physics,” *PTEP*, vol. 2022, p. 083C01, 2022. doi: 10.1093/ptep/ptac097.
- [41] L Garren, I. Knowles, T Sjöstrand, and T Trippe, “Monte carlo particle numbering scheme,” *The European Physical Journal. C, Particles and Fields.*, vol. 15, no. 1-4, pp. 205–207, 2000.

Supplementary Code

A.1 Header File

```
1  /*- Defining all variables -*/
2
3 // Modifiables
4 const int event_count = 1000; // Sets maximum
5
6 // Set modifiables
7 const int wwe_range = 1000;
8 const int wwp_range = 1000;
9 float w1phi_com_selected = 0.0;
10
11 // Constants
12 const float invariant_mass = 13000; const float w_mass = 80.318; const
13     float p_mass = 0.938272;
14
15 // Scalars
16 double px, py, pz, energy, mass;
17 int pid, c1,c2,c3,c4,c5,c6,c7;
18 int direction_parameter;
19 float wwpz_lab, wwe_lab;
20 float l1w1_angle_lab_candidate, l2w2_angle_lab_candidate;
21 float daw1, daw2;
22 float wp_candidate[6];
23 float w1px_com_selected, w1py_com_selected;
24 float w1phi_selected;
25 float w1phi_lab, w2phi_lab;
26 float w1pxy_lab, w2pxy_lab;
27 float successRate;
28 int number_of_candidates;
29 float phi_increment;
30 int max_events;
31
32 double particle_lab[6][4][event_count];
33 double w1px_lab_event; double w1py_lab_event; double w1pz_lab_event;
34     double w1e_lab_event;
35 double w2px_lab_event; double w2py_lab_event; double w2pz_lab_event;
36     double w2e_lab_event;
37 double p1px_lab_event; double p1py_lab_event; double p1pz_lab_event;
38     double p1e_lab_event;
39 double p2px_lab_event; double p2py_lab_event; double p2pz_lab_event;
40     double p2e_lab_event;
41 double l1px_lab_event; double l1py_lab_event; double l1pz_lab_event;
42     double l1e_lab_event;
```

```
37 double l2px_lab_event; double l2py_lab_event; double l2pz_lab_event;
38     double l2e_lab_event;
39
40 float wwp_com;
41 float wwe_com;
42 float w1_gamma, w1_beta;
43 float w2_gamma, w2_beta;
44 float w1px_lab, w1py_lab, w1pz_lab;
45 float w2px_lab, w2pz_lab, w2py_lab;
46 float w1e_lab, w2e_lab;
47 float wwe_diff;
48 float l1w1_angle_lab, l2w2_angle_lab;
49 string print_location;
50
51 // Vectors
52 std::vector<float> vector_w1phi_lab_candidate,
53     vector_w2phi_lab_candidate;
54 std::vector<float> vector_w1w1, vector_w2w2,
55 std::vector<float> daw1_all, daw2_all;
56 std::vector<float> daw1_all_out, daw2_all_out, successRate_out, repeats,
57     time_out;
58 std::vector<std::vector<float>> vector_wp_lab_candidate(6, std::vector<
59     float>());
60 std::vector<std::vector<float>> wp_ref(3, std::vector<float>());
61
62 std::vector<float> sd1;
63 std::vector<float> sd2;
64 std::vector<float> mean1;
65 std::vector<float> mean2;
66
67 // ROOT Arrays
68 ROOT::Math::PxPyPzEVector w1_lab, w2_lab, p1_lab, p2_lab, l1_lab, l2_lab
69     ;
70 ROOT::Math::PxPyPzEVector w1_lab_average, w2_lab_average;
71 ROOT::Math::PxPyPzEVector w1_com, w2_com, ww_com, w1_lab_ref, w2_lab_ref
72     ;
73 ROOT::Math::DisplacementVector3D<ROOT::Math::Cartesian3D<double>, ROOT::
74     Math::DefaultCoordinateSystemTag> w1_angle_diff, w2_angle_diff;
75 ROOT::Math::DisplacementVector3D<ROOT::Math::Cartesian3D<double>, ROOT::
76     Math::DefaultCoordinateSystemTag> w1_unit_distance_lab,
77     w2_unit_distance_lab;
78 ROOT::Math::DisplacementVector3D<ROOT::Math::Cartesian3D<double>, ROOT::
79     Math::DefaultCoordinateSystemTag> w1_unit_distance_lab_ref,
80     w2_unit_distance_lab_ref;
81 ROOT::Math::DisplacementVector3D<ROOT::Math::Cartesian3D<double>, ROOT::
82     Math::DefaultCoordinateSystemTag> l1_unit_distance_lab,
83     l2_unit_distance_lab;
84 ROOT::Math::PxPyPzEVector w1_lab_candidate, w2_lab_candidate;
85 ROOT::Math::BoostZ wz_boost;
```

A.2 Styling File

```
1 const std::string currentDateTime() {
2
3     time_t      now = time(0);
4     struct tm  tstruct;
```

APPENDIX A. SUPPLEMENTARY CODE

```
5     char          buf [80];
6     tstruct = *localtime(&now);
7     strftime(buf, sizeof(buf), "%Y-%m-%d--%H-%M-%S", &tstruct);
8     return buf;
9     cout << currentDateTime() << endl;
10    }

11
12 string format_plots(int event_max){
13
14     std::string print_location = "/Users/Username/Simulation/Results/
15         Plots_"+currentDateTime()+"";
16     int result = mkdir(print_location.c_str(), 0777);
17
18     TFile *f = TFile::Open("/Users/Username/Simulation/Simulation_Output
19         .root");
20     TTree *t = (TTree*)f->Get("w1w2");

21     float line_width = 2;
22     gStyle->SetOptStat("emr");
23     gStyle->SetStatW(0.15);
24     gStyle->SetStatH(0.1);
25     gStyle->SetStatY(0.88);
26     gStyle->SetStatX(0.88);
27     gStyle->SetStatFontSize(0.03);

28     gROOT->SetBatch(TRUE);
29
30     Int_t color;
31     color = TColor::GetColor("#6C8EBF");
32
33 /***** W1 *****/
34
35     TCanvas *canvas = new TCanvas("canvas", "", 0, 0, 450, 700);
36     canvas->Divide(2,3);
37
38     /*-----W1PX-----*/
39     canvas->cd(1);
40     TH1D * plot_w1px = new TH1D("plot_w1px","", 80, -400, 400);
41
42     gPad->SetBottomMargin(0.1);
43     plot_w1px->SetFillStyle(3002);
44     plot_w1px->SetFillColor(color2);
45     plot_w1px->GetXaxis()->SetTitle(" W1 X-Momentum (GeV/c) ");
46     plot_w1px->GetYaxis()->SetTitle(" Events ");
47     plot_w1px->GetYaxis()->SetRangeUser(0,event_max);
48     plot_w1px->Draw("");
49     plot_w1px->SetLineWidth(line_width);
50     plot_w1px->SetLineColor(color);

51
52     t->Project("plot_w1px", "w1px_candidate");
53     string file_name_1 = "plot_w1px.pdf";
54
55     /*-----W1PY-----*/
56     canvas->cd(3);
57     TH1D * plot_w1py = new TH1D("plot_w1py", "", 80, -400, 400);
58
59     gPad->SetBottomMargin(0.1);
60     plot_w1py->SetFillStyle(3002);
```

APPENDIX A. SUPPLEMENTARY CODE

```
61 plot_w1py->SetFillColor(color2);
62 plot_w1py->GetXaxis()->SetTitle(" W1 Y-Momentum (GeV/c) ");
63 plot_w1py->GetYaxis()->SetTitle(" Events ");
64 plot_w1py->GetYaxis()->SetRangeUser(0,event_max);
65 plot_w1py->Draw("");
66 plot_w1py->SetLineWidth(line_width);
67 plot_w1py->SetLineColor(color);

68
69 t->Project("plot_w1py", "w1py_candidate");
70 string file_name_2 = "plot_w1py.pdf";
71
72 /*-----W1PZ-----*/
73 canvas->cd(5);
74 TH1D * plot_w1pz = new TH1D("plot_w1pz", "", 80, -400, 400);

75 gPad->SetBottomMargin(0.1);
76 plot_w1pz->SetFillStyle(3002);
77 plot_w1pz->SetFillColor(color2);
78 plot_w1pz->GetXaxis()->SetTitle(" W1 Z-Momentum (GeV/c) ");
79 plot_w1pz->GetYaxis()->SetTitle(" Events ");
80 plot_w1pz->GetYaxis()->SetRangeUser(0,event_max);
81 plot_w1pz->Draw("");
82 plot_w1pz->SetLineWidth(line_width);
83 plot_w1pz->SetLineColor(color);

84
85 t->Project("plot_w1pz", "w1pz_candidate");
86 string file_name_3 = "plot_w1pz.pdf";
87
88 /****** W2 ******/
89
90 /*-----W2PX-----*/
91 canvas->cd(2);
92 TH1D * plot_w2px = new TH1D("plot_w2px", "", 80, -400, 400);

93 gPad->SetBottomMargin(0.1);
94 plot_w2px->SetFillStyle(3002);
95 plot_w2px->SetFillColor(color2);
96 plot_w2px->GetXaxis()->SetTitle(" W2 X-Momentum (GeV/c) ");
97 plot_w2px->GetYaxis()->SetTitle(" Events ");
98 plot_w2px->GetYaxis()->SetRangeUser(0,event_max);
99 plot_w2px->Draw("");
100 plot_w2px->SetLineWidth(line_width);
101 plot_w2px->SetLineColor(color);

102
103 t->Project("plot_w2px", "w2px_candidate");
104 string file_name_5 = "plot_w2px.pdf";
105
106
107 /*-----W2PY-----*/
108 canvas->cd(4);
109 TH1D * plot_w2py = new TH1D("plot_w2py", "", 80, -400, 400);

110 gPad->SetBottomMargin(0.1);
111 plot_w2py->SetFillStyle(3002);
112 plot_w2py->SetFillColor(color2);
113 plot_w2py->GetXaxis()->SetTitle(" W2 Y-Momentum (GeV/c) ");
114 plot_w2py->GetYaxis()->SetTitle(" Events ");
115 plot_w2py->GetYaxis()->SetRangeUser(0,event_max);
116 plot_w2py->Draw("");
```

APPENDIX A. SUPPLEMENTARY CODE

```
119 plot_w2py->SetLineWidth(line_width);
120 plot_w2py->SetLineColor(color);
121
122 t->Project("plot_w2py", "w2py_candidate");
123 string file_name_6 = "plot_w2py.pdf";
124
125 /*-----W2PZ-----*/
126 canvas->cd(6);
127 TH1D * plot_w2pz = new TH1D("plot_w2pz", "", 80, -400, 400);
128
129 gPad->SetBottomMargin(0.1);
130 plot_w2pz->SetFillStyle(3002);
131 plot_w2pz->SetFillColor(color2);
132 plot_w2pz->GetXaxis()->SetTitle(" W2 Z-Momentum (GeV/c) ");
133 plot_w2pz->GetYaxis()->SetTitle(" Events ");
134 plot_w2pz->GetYaxis()->SetRangeUser(0,event_max);
135 plot_w2pz->Draw("");
136 plot_w2pz->SetLineWidth(line_width);
137 plot_w2pz->SetLineColor(color);
138
139 t->Project("plot_w2pz", "w2pz_candidate");
140 string file_name_7 = "plot_w2pz.pdf";
141
142 canvas->Print((print_location + "combined_plots.pdf").c_str());
143
144 /****** DAW *****/
145
146 TCanvas *canvasd = new TCanvas("canvas", "", 0, 0, 500, 200);
147
148 canvasd->Divide(2,1);
149
150 /*-----DAW 1-----*/
151 canvasd->cd(1);
152 TH1D * plot_daw1 = new TH1D("plot_daw1", "", 80, 0, 1);
153
154 plot_daw1->GetXaxis()->SetTitle(" W1 reconstruction difference (Rad)");
155 plot_daw1->GetYaxis()->SetTitle(" Events ");
156 plot_daw1->GetYaxis()->SetRangeUser(0,150);
157 plot_daw1->SetFillColor(color2);
158 plot_daw1->Draw("");
159 plot_daw1->SetLineWidth(line_width);
160 plot_daw1->SetLineColor(color);
161
162 t->Project("plot_daw1", "daw1");
163 string file_name_4 = "plot_daw1.pdf";
164
165 mean1.push_back(plot_daw1->GetMean());
166 sd1.push_back(plot_daw1->GetStdDev());
167
168 /*-----DAW 2-----*/
169 canvasd->cd(2);
170 TH1D * plot_daw2 = new TH1D("plot_daw2", "", 80, 0, 1);
171
172 plot_daw2->GetXaxis()->SetTitle(" W2 reconstruction difference (Rad)");
173 plot_daw2->GetYaxis()->SetTitle(" Events ");
174 plot_daw2->GetYaxis()->SetRangeUser(0,150);
```

APPENDIX A. SUPPLEMENTARY CODE

```
175 plot_daw2->SetFillColor(color2);
176 plot_daw2->Draw("");
177 plot_daw2->SetLineWidth(line_width);
178 plot_daw2->SetLineColor(color);
179
180 t->Project("plot_daw2", "daw2");
181 string file_name_8 = "plot_daw2.pdf";
182
183 canvasd->Print((print_location + "combined_daw_plots.pdf").c_str());
184
185 mean2.push_back(plot_daw2->GetMean());
186 sd2.push_back(plot_daw2->GetStdDev());
187
188 cout << "***" << endl;
189 cout << "Plotting generation successful." << endl;
190 cout << "***" << endl;
191
192 return print_location;
193 }
194
195 int format_plots_averages(string print_location, const std::vector<float>& x, const std::vector<float>& s, const std::vector<float>& time_out) {
196
197 float line_width = 3;
198 float label_value = 0.02;
199
200 gROOT->SetStyle("Modern");
201 gROOT->SetBatch(TRUE);
202 gROOT->ForceStyle();
203
204 Int_t color;
205 color = TColor::GetColor("#6C8EBF");
206
207 string parameter_name = "Parameter name";
208
209 TCanvas *canvasmean = new TCanvas("canvasmean", "", 0, 0, 180, 150);
210 TGraph* graph_mean1 = new TGraph(x.size(), &x[0], &mean1[0]);
211 TGraph* graph_mean2 = new TGraph(x.size(), &x[0], &mean2[0]);
212 gPad->SetLeftMargin(0.2);
213 graph_mean1->SetTitle("");
214 graph_mean1->GetXaxis()->SetTitle(parameter_name.c_str());
215 graph_mean1->GetYaxis()->SetTitle("Mean of angle differences (Rad)");
216 ;
217 graph_mean1->SetLineWidth(line_width);
218 graph_mean1->SetLineColor(color2);
219 graph_mean1->SetMarkerColor(color2);
220 graph_mean1->SetMarkerStyle(21);
221 graph_mean1->SetMarkerSize(0.3);
222 graph_mean1->GetXaxis()->SetLabelSize(label_value);
223 graph_mean1->GetYaxis()->SetRangeUser(0,0.3);
224 graph_mean1->Draw("");
225
226 gPad->SetLeftMargin(0.2);
227 graph_mean2->SetLineWidth(line_width);
228 graph_mean2->SetLineColor(kBlack);
229 graph_mean2->SetMarkerColor(kBlack);
230 graph_mean2->SetMarkerStyle(21);
```

APPENDIX A. SUPPLEMENTARY CODE

```
230 graph_mean2->SetMarkerSize(0.3);
231 graph_mean2->GetXaxis()->SetLabelSize(label_value);
232 graph_mean2->GetYaxis()->SetRangeUser(0,0.5);
233 graph_mean2->Draw("PL");
234
235 auto legend_p = new TLegend(0.8, 0.8, 0.9, 0.9);
236 legend_p->AddEntry(graph_mean1, "W1", "l");
237 legend_p->AddEntry(graph_mean2, "W2", "l");
238 legend_p->SetEntrySeparation(0.1);
239 legend_p->SetMargin(0.5);
240 legend_p->Draw();
241 canvasmean->Print((print_location + "graph_mean.pdf").c_str());
242
243 ****
244
245 TCanvas *canvassd = new TCanvas("canvassd", "", 0, 0, 180, 150);
246 TGraph* graph_sd1 = new TGraph(x.size(), &x[0], &sd1[0]);
247 TGraph* graph_sd2 = new TGraph(x.size(), &x[0], &sd2[0]);
248 gPad->SetLeftMargin(0.2);
249 graph_sd1->SetTitle("");
250 graph_sd1->GetXaxis()->SetTitle(parameter_name.c_str());
251 graph_sd1->GetYaxis()->SetTitle("Standard deviation of angle
252 differences (Rad)");
253 graph_sd1->SetLineWidth(line_width);
254 graph_sd1->SetLineColor(color2);
255 graph_sd1->SetMarkerColor(color2);
256 graph_sd1->SetMarkerStyle(21);
257 graph_sd1->SetMarkerSize(0.3);
258 graph_sd1->GetXaxis()->SetLabelSize(label_value);
259 graph_sd1->GetYaxis()->SetRangeUser(0,0.5);
260 graph_sd1->Draw("");
261
262 gPad->SetLeftMargin(0.2);
263 graph_sd2->SetLineWidth(line_width);
264 graph_sd2->SetLineColor(kBlack);
265 graph_sd2->SetMarkerColor(kBlack);
266 graph_sd2->SetMarkerStyle(21);
267 graph_sd2->SetMarkerSize(0.3);
268 graph_sd2->GetXaxis()->SetLabelSize(label_value);
269 graph_sd2->GetYaxis()->SetRangeUser(0,0.3);
270 graph_sd2->Draw("PL");
271
272 auto legend_sd = new TLegend(0.8, 0.8, 0.9, 0.9);
273 legend_sd->AddEntry(graph_sd1, "W1", "l");
274 legend_sd->AddEntry(graph_sd2, "W2", "l");
275 legend_sd->SetEntrySeparation(0.1);
276 legend_sd->SetMargin(0.5);
277 legend_sd->Draw();
278 canvassd->Print((print_location + "graph_sd.pdf").c_str());
279
280 ****
281
282 TCanvas *canvas_time = new TCanvas("canvas_time", "", 0, 0, 150,
283 150);
284 TGraph* graph_time = new TGraph(x.size(), &x[0], &time_out[0]);
285 gPad->SetLeftMargin(0.2);
286 graph_time->SetTitle("");
287 graph_time->GetXaxis()->SetTitle(parameter_name.c_str());
```

APPENDIX A. SUPPLEMENTARY CODE

```
286 graph_time->GetYaxis()->SetTitle("Run time (ms)");
287 graph_time->SetLineWidth(line_width);
288 graph_time->SetLineColor(color2);
289 graph_time->SetMarkerStyle(21);
290 graph_time->GetXaxis()->SetLabelSize(label_value);
291 graph_time->SetMarkerSize(0.3);
292 graph_time->Draw("");
293 canvas_time->Print((print_location + "graph_runtime.pdf").c_str());
294
295 TCanvas *canvas_success = new TCanvas("canvas_success", "", 0, 0,
296 150, 150);
297 TGraph* graph_success = new TGraph(x.size(), &x[0], &s[0]);
298 gPad->SetLeftMargin(0.2);
299 graph_success->SetTitle("");
300 graph_success->GetXaxis()->SetTitle(parameter_name.c_str());
301 graph_success->GetYaxis()->SetTitle("Success rate (%)");
302 graph_success->SetLineWidth(line_width);
303 graph_success->SetLineColor(color2);
304 graph_success->SetMarkerStyle(21);
305 graph_success->GetXaxis()->SetLabelSize(label_value);
306 graph_success->SetMarkerSize(0.3);
307 graph_success->Draw("");
308 canvas_success->Print((print_location + "graph_success.pdf").c_str()
309 );
310
311
312 %
```

Agenda and Minutes

1st Meeting Minutes

Meeting Date: 13/01/23.

Location: Zoom (online), meeting recording can be found here - password is
\$J0^X9K4

Present : Rishabh Lassen, Rishi Kalra, Joe George, Priya Dhami, Swathi Nambiar, Ashik Rahman, Jocelyn Japnanto, Aileene Wang.

Apologies: None.

In attendance: None.

The Chair: Mario Campanelli.

Minute Taker(s): Rishabh Lassen, Jocelyn Japnanto.

Agenda:

The primary objective of the meeting is to establish a rapport with the board member and accomplish the following tasks:

1. Discuss preliminary readings and questions from project brief with Mario.
2. Discuss final aims and objectives to achieve during the course of the project.
3. Discuss a rough time plan to ensure the successful delivery of the report and poster before the deadlines.
4. Collect resources for the literature review.

Start Time: 13:00.

Meeting Log:

Introduction and Project Brief:

- Everyone: introduces themselves and Mario speaks about his life in Geneva.

APPENDIX B. AGENDA AND MINUTES

- Mario: gave a presentation which introduced CERN, ATLAS and AFP.
- Mario: gave a second presentation which introduced the context of the project including proton-proton collisions and relevant Feynman diagrams representing the WW boson production from pp collision.
- Rishabh: gave an introduction into the background research that had been carried out prior to meeting.
- Mario: explains the general intuition behind how the code is trying to reconstruct the WW boson directions and recommends that the group should first try to understand the code and then begin to make it efficient and optimise some of the parameters (unknown at the time).
- Joe: asks when we will receive the code.
- Mario: says he will try to send the code by the end of next week.

Project Organisation:

- Priya: initially proposed that we should split the group into two sub-groups: those who run and simulate the events and those who rewrite the code to find possible improvements - this was not finalised.
- Swathi: clarified that our aim is to test the code to see that it indeed behaves correctly and to see how modifications can affect the precision of measurements.
- Rishi: recommended that we should use "Notion" to organise our group project going forward and that we should look into producing a Gantt Chart.
- Mario: gave suggested literature titled "*Reconstruction of the W boson directions in fully leptonic decays $WW \rightarrow l\nu l\nu$ at ATLAS Forward Proton*" to read for further context.

Meeting Conclusions and Aims for Next Session:

- We decided to use Notion for our organisation.
- For next week, the aim is to read the paper and the code (once received).

Meeting End Time: 14:47.

Board Member Feedback:

- You're off to a good start so keep up the good work!
- To contribute to the literature review, ensure that everyone reads about given paper.
- The more effort you all invest in reading and conducting careful experiments/simulations, the better your project's outcome will be.
- Remember that teamwork is a crucial part of this course, and enjoy collaborating with your team.
- Enjoy conducting the coding and have fun with the process.

2nd Meeting Minutes

Meeting Date: 20/01/23.

Location: Zoom (online), meeting recording can be found here - password is @5nt3#K9

Present : Rishabh Lassen, Rishi Kalra, Joe George, Priya Dhami, Swathi Nambiar, Ashik Rahman, Jocelyn Japnanto, Aileene Wang.

Apologies: None.

In attendance: None.

The Chair: Rishabh Lassen.

Minute Taker(s): Rishabh Lassen, Jocelyn Japnanto.

Agenda:

Main Objective: Provide an update on the progress made so far and outline the steps that we will take to complete the necessary requirements to run the code.

Discussion Points:

1. Discuss readings and questions from paper given in previous meeting with Mario.
2. Setup ROOT to open code.
3. Run the code for the first time and get a break down of structure.

Start Time: 11:00.

Meeting Log:

Progress Update:

- Rishabh: gave a general explanation of our current understanding of the literature that was given in the previous meeting, as well as overall project aims.
- Mario: verified understanding and suggests the group should spend the time in the meeting to open and run the code.

Installing ROOT:

- Mario directs everyone to "<https://root.cern.ch/>" and asks whether anyone has a UNIX or Linux machine.
- Rishabh: suggested that since it is easier to set up on a Macintosh system, we should let the team members with a Mac computer go through the set-up process first, so we can get the code running as soon as possible. Rishabh then shares his screen to walk through the website to install ROOT.

APPENDIX B. AGENDA AND MINUTES

- Rishabh: navigated to the webpage and attempts to download by running *brew install root* in terminal as suggested by website.
- Mario: said to install ROOT via *Homebrew* first.
- Rishabh: navigated to the Homebrew webpage and attempts to download the package manager. Troubleshooting errors were encountered.
- Mario: recommended contacting PhD student Yi He who wrote the code that the project intends to test and run. The following email was given (*yi.he@cern.ch*).
- Mario: gave a demo of the code on his remote CERN machine to save time due to delayed downloading.

Next Steps:

- Mario: concluded by recommending to watch tutorials online to download ROOT on Windows systems and to contact Yi He to explain the code and answer any other questions related to it. Mario then left the call.
- Priya: recommended that we should instead split into a theory and coding group.
- Everyone: agreed with the idea.
- Aileene, Jocelyn, Priya, Ashik: expressed to join theory team.
- Rishabh, Swathi, Joe, Rishi: expressed to join coding team.
- Aileene, Jocelyn: decided to begin conducting research on the AFP detector.
- Priya, Ashik: decided to begin conducting research on the W boson and relevant physics literature.
- Swathi: stated that the literature review should include the research that will be conducted and that they should make notes to help them write it.
- Rishi: set up the Notion page, ensured access was granted to all team members to begin uploading resources.

Meeting Conclusions and Aims for Next Session:

- Coding team should continue to try and install ROOT onto their systems.
- Theory team should begin conducting research on their allocated areas and make notes on them to aid with writing the literature review.

Meeting End Time: 12:32.

Board Member Feedback:

- The team appears to be serious and well-organised and the minutes are being submitted on time.

APPENDIX B. AGENDA AND MINUTES

- The project has progressed as expected so far, but the next few weeks will be crucial for making significant progress.
- It is recommended to try and install ROOT via homebrew or any other method that may seem easier.
- Recommended literature should be read and understood to prepare writing the literature review.

3rd Meeting Minutes

Meeting Date: 03/02/23.

Location: Zoom (online), meeting recording can be found here - password is
=nTf+51=

Present : Rishabh Lassen, Rishi Kalra, Joe George, Priya Dhami, Swathi Nambiar, Ashik Rahman, Jocelyn Japnanto, Aileene Wang.

Apologies: None.

In attendance: None.

The Chair: Rishabh Lassen.

Minute Taker(s): Rishabh Lassen.

Agenda:

Main Objective: Provide an update on the progress made so far and discuss technicalities of the code including a clarification of the task.

Discussion Points:

1. Discussion of potential breakdown of the final report.
2. Allocation and designation of responsibilities for writing the executive summary.
3. Discussion of current status of code understanding after having met with Yi.
4. Discussion of potential avenues for code optimisation.

Start Time: 14:00.

Meeting Log:

Coding Team:

- Joe: broke down his understanding of various sections of the code and asked about meaning/purpose of the following variables: *ewwlab*, *EP1*, *EP2*, *P1*.
- Mario: responded by highlighting that *ewwlab* is energy of the two *W* bosons in the lab frame, *EP1* is the energy of the first proton, *EP2* is the energy of the second, and *P1* is the Lorentz vector for the first proton.
- Rishabh: showed that the code was running on his system and visualised the plots that the code produced including the distribution of the individual Cartesian momentum components of the reconstructed *W* bosons using "*TBrowser t*".
- Mario: questioned why there were only a few data points.

APPENDIX B. AGENDA AND MINUTES

- Joe: explained that the number of events had been reduced so that the code could run faster whilst it was being interpreted.

Theory Team:

- Aileene, Jocelyn: confirmed that they had almost finished the research on their delegated areas and made notes on a shared Google document.
- Ashik, Priya: also confirmed that they had almost finished.

Questions:

- Priya: asked whether our interaction demonstrates quadrilinear gauge coupling since it was a term she found during the research that she was unsure of.
- Mario: highlighted that it refers to the coupling between four gauge bosons, which are particles that mediate the fundamental forces of nature and was not of interest in this interaction.
- Swathi: asked what parameters could be "optimised".
- Mario: several parameters can be changed for example the precision of the angular detection of the code, the threshold for energy differences between the reconstructed energies and the measured energies. Valphi, ValEww, and ValRp can also be varied too.
- Joe: asked how efficiency can be quantified since the instructions simply say to "improve efficiency" very vaguely.
- Mario: performance can be quantified by looking at the plot between the angle difference deviations of the reconstruction and measured angles – ideally it should be a sharp peak around zero.

Final Report Introduction Breakdown:

- Jocelyn: asked how the final report can be broken down.
- Mario: Possible sections could include the LHC, ATLAS detector, AFP, code structure, schematics, and description of the code – nothing technical (code searches for all possible candidates, then it makes a boost, then it calculates the Lorentz boost from the energy etc...)

Meeting Conclusions and Aims for Next Session:

- Continue to go through the code and make comments explaining the purpose of sections in the code and relate them back to what is happening mathematically.
- Start to look through the code and identify variables that could be changed to investigate their impact on performance/efficiency.
- Theory team should begin writing the literature review using their notes.

Meeting End Time: 16:50.

Board Member Feedback:

- The team appears to be a little slow in the progress of understanding the code, more meetings should be held with Yi to bring them up to speed.
- Try to save questions about code technicalities for Yi and ask questions about theory and other concerns with myself (Mario).
- Theory team should start thinking about starting to write up the literature review.
- Decide on the general structure for the final report as a group and create a break down.
- Overall keep up the hard work!

4th Meeting Minutes

Meeting Date: 11/02/23.

Location: Zoom (online), meeting recording can be found here - password is V?Z60Yid

Present : Rishabh Lassen, Rishi Kalra, Joe George, Priya Dhami, Swathi Nambiar, Ashik Rahman, Jocelyn Japnanto, Aileene Wang.

Apologies: None.

In attendance: Yi He.

The Chair: Rishabh Lassen.

Minute Taker(s): Rishabh Lassen.

Agenda:

Main Objective: Provide an update on the progress made so far, discuss the plan for the report and verify plans with code development.

Discussion Points:

1. Review proposed report structure with board member.
2. Request clarification on project direction.
3. Update Mario about the code progression and implementation of functions to simplify the code ready to change the variables.
4. Confirm uses of functions to split up code and use of global variables.
5. Ask about effective field theory and more details on how to incorporate this properly into the report - clarify the code results and their impact on physics beyond the standard model.

Start Time: 12:00.

Meeting Log:

Recap of Proposed Report Breakdown:

- Rishabh: gave a general explanation of the suggested breakdown: include the LHC, ATLAS detector, AFP. For the main body: how the code works intuitively, improving code efficiency and clearing redundant variables, the purpose of individual functions, optimised parameters and their resulting effects on code outputs.

Addition of SMEFT to Theory Section:

APPENDIX B. AGENDA AND MINUTES

- Mario: agreed with the suggested breakdown and added that *standard model effective field theory (SMEFT)* can be mentioned in the introduction and conclusion to demonstrate physics beyond the standard model and how the reconstructed angle can be used to constrain the *SMEFT* - this should not be a heavily emphasised part of the report.

Interpreting Code Results:

- Rishabh: asked what is expected for the "most optimal" code, is one candidate supposed to survive the entire selection process?
- Yi: replied that ideally, it is possible, but since there are many events and simulations, more than one event will survive the selection process and so the code can yield the "same angle" but to different precision which could be considered to be within an uncertainty of one another and actually represent the same interaction.
- Mario: added that if there is one cluster of results, i.e. many solutions close to each other, the average for the direction angle should be taken as a solution. However, if there are many distinct clusters of directions, the average should be taken for each cluster and reported as different possible solutions.

Code Output:

- Joe: displayed code to Mario to present current code status and discussed the output plots of W boson momenta.
- Mario: confirmed they are correct and that the total momentum in the z -direction for the W boson will be the sum of the momenta of the two individual protons.

Theory Team Questions:

- Ashik: asked how much emphasis should be given to physics beyond the SM in the report.
- Mario: responded that it shouldn't be a large part of the report.

Linking Theory and Code:

- Priya: suggested that someone from the theory team should begin to read the code and associate the theory from their readings to the code to help with writing about the code in the report.
- Everyone: responded that it was a good idea.

Meeting Conclusions and Aims for Next Session:

- Theory team should decide who will write the code-theory linking document.
- Coding team should think about clustering methods in ROOT and how to implement them.
- Delegation of poster-related responsibilities.

Meeting End Time: 12:47.

Board Member Feedback:

- Continue to work on the code and start writing other sections of the report to ensure finishing on time!
- Start thinking about what things are key and should be added to the poster.

5th Meeting Minutes

Meeting Date: 01/03/23.

Location: Physics Building D17.

Present : Rishabh Lassen, Rishi Kalra, Joe George, Priya Dhami, Ashik Rahman, Jocelyn Japnanto, Aileene Wang.

Apologies: Swathi Nambiar (fever).

In attendance: None.

The Chair: Rishabh Lassen.

Minute Taker(s): Rishabh Lassen.

Agenda:

Main Objective: Provide an update on the progress made so far, get feedback the current status of the report and verify plans for clustering.

Discussion Points:

1. Presentation of code plot outputs and discussion of current code status.
2. Clarification of implementing clustering of solutions - is k-means clustering the best method?
3. Clarification on interpreting 3D plots of W momenta.
4. Clarification of the level of detail required in the theory section of the report, specifically how much to write about the broader picture of the standard model.
5. Discussion on the impact of changing the angle cut for lepton decay angle to an angle greater than 2π - is another peak expected?
6. Importance of pseudorapidity and whether it is relevant enough for the report.
7. Recommended referencing style for the report.
8. How much of the code should be included in the report - should it be a breakdown of each individual component in a section?
9. Presentation of the report.

Start Time: 17:04.

Meeting Log:

The Standard Model in Theory:

- Joe: asked how much detail should the report go into about the standard model?

APPENDIX B. AGENDA AND MINUTES

- Mario: briefly talk about the standard model/fundamental forces. Do not spend too much on this because it is not directly relevant to the project and could be considered as padding.
- Ash: asked if the Higgs boson should be mentioned in the section.
- Mario: replied it is not necessary.

Update on Code Status:

- Joe: displayed that the code now stores all of the plots onto the same pdf which can be used to easily see the differences between the outputs of the codes for different input variables.
- Joe: displayed how the parameters change the reconstruction rate.
- Mario: the reconstruction rate shows how many candidates are successful.

Solution Clustering:

- Mario: asked if clustering had been implemented.
- Joe: explains how this has been looked into and k-means clustering seems to be a machine learning technique which can carry this out.
- Mario: reiterated that the average between two clusters will not be the correct solution.
- Mario: check to see if the average solution satisfies your cuts. If it does, accept it and if not (the average does not pass the cuts) then remove the solution that is furthest away from the average. Take the average of all the clusters, then remove the solution that is furthest away, then take the average of the remaining clusters and then remove the furthest solution. Repeat until you get one solution that works.
- Joe: asked what is the ideal combination of success rate and deviation.
- Mario: the success rate should be greater than 50% and the averaging should reduce the tails of the plot of the deviations between truth-value angle and the observed angle.

Pseudorapidity:

- Joe: asked whether pseudorapidity should be included in the format.
- Mario: if it is not in the code, do not mention it.

Report Referencing style and Flow Chart:

- Jocelyn: asked Joe to present the flow chart for the codes structure.
- Mario: confirms that it is good.
- Rishabh: asked what referencing style should be used for the report.

APPENDIX B. AGENDA AND MINUTES

- Mario: use JHEP style.
- Joe: asked whether the theory should be linked to the code throughout the report.
- Mario: if the function includes an equation then talk about the maths more than the code itself.
- Joe: asked if smearing be mentioned in the report since it has been added to the report?
- Mario: yes of course. - Joe: asked if the WW decay section in the report should be merged with the standard model.
- Mario: if you want to.

Next Steps Section of the Report and Code:

- Joe: mentioned that Yi suggested to add more cuts to the code for the selection process and asked what other cuts could be implemented.
- Mario: other cuts are not necessary and may not even be meaningful.
- Rishabh: asked what would be the next steps of the project so that it can be written in the report.
- Mario: consider the W mass as a distribution and not as a constant.

Meeting Conclusions and Aims for Next Session:

- Coding team should attempt to implement k-means clustering or some alternative method which can handle multiple solutions.
- Jocelyn, Rishabh and Aileene should arrange to begin making the poster.
- Theory section of the report should be updated with respect to the given feedback.

Meeting End Time: 17:55.

Board Member Feedback:

- Start writing up the results and analysis sections of the report and begin the poster.

6th Meeting Minutes

Meeting Date: 15/03/23.

Location: Zoom (online), meeting was not recorded.

Present : Rishabh Lassen, Rishi Kalra, Joe George, Priya Dhami, Ashik Rahman, Jocelyn Japnanto, Aileene Wang, Swathi Nambiar.

Apologies: None.

In attendance: None.

The Chair: Rishi Kalra.

Minute Taker(s): Rishi Kalra, Rishabh Lassen.

Agenda:

Main Objective: Present the new averaging mechanism and verify the findings as a result of its implementation. Start shifting focus to the poster.

Discussion Points:

1. Presentation of the poster and recommendations on the word-to-figure ratio.
2. Presentation of the final results with the new averaging mechanism and discussion on what are the key things that should be included in the analysis.
3. Confirmation of the larger scale significance of the project - to be included in the executive summary.
4. Discussion of how SMEFT ties into the significance of the project specifically.

Start Time: 10:01.

Meeting Log:

Presentation of Poster:

- Rishabh: presented the poster and described the structure including a brief breakdown of the following sections: the introduction, the ATLAS AFP detector, the W boson decay and the reconstruction of the kinematic process.
- Mario: the poster has a nice structure and the flow chart is particularly nice. However, as well as the Feynman diagram, there should be a diagram that shows the lepton decay angle cones and the azimuthal parameter to show the event that is being constructed. This is the most crucial part and should be present in the poster. The poster should have more emphasis on the reconstruction method and the amount of text should be somewhat reduced to make it visually more pleasing.

The New Averaging Mechanism:

APPENDIX B. AGENDA AND MINUTES

- Joe: displayed the code which runs the new averaging mechanism and described how the average of the surviving candidates passes through the same selection process as before and the candidate which deviates the most from the average is removed until the average satisfies the energy and lepton decay angle cuts.
- Mario: that is exactly the process that was planned, the candidate must pass the cuts as was shown so well done on that.
- Joe: presented the final plots showing how the changes in the parameters such as the azimuthal increment size can lead to increased reconstruction rate but also decreased efficiency.
- Mario: that is good but what does the WW direction plot look like?
- Joe: presented the angle reconstruction difference of the two bosons and how the new averaging mechanism leads to a sharper and more narrower peak.
- Mario: this is again what is expected to be observed.
- Joe: questioned why the new averaging mechanism doesn't eliminate the tail completely and leave just one or a few candidates.
- Priya: mentioned that this could be occasions where there are just single one-off events that make it through.

Result and Analysis in the Report:

- Rishabh: asked much should the results of the old code be emphasised in the report.
- Mario: no need to go in detail, just quote the results and use of old code. If new averaging approach is much better, there is no point in showing/talking about the old one.
- Mario: If new average approach is much better, no point showing the old one.
- Rishabh: suggested that the original averaging mechanism plots can be shown, rather than having in two different sections, and then talk about the parameters that were changed for the new code and compare to the old code as a baseline. Overall, aim to talk about the new one over the old one.

Project Significance for Executive Summary in the Report:

- Rishabh and Rishi: asked what the bigger picture significance of the project is?
- Mario: the reconstruction of W s can help remove background and improves the limits with coupling (EFT), it is another variable that you can measure.
- Jocelyn: asked about the AFP relevance on understanding electroweak theory.
- Mario: details the new information given by AFP that helps reconstruction.

Report Referencing style and Structure:

APPENDIX B. AGENDA AND MINUTES

- Priya: asked how should the original WWREC paper be referenced if it was not published.
- Mario: it is original work so it does not need to be referenced.
- Rishabh: asked if the entire style of the report be JHEP or does it not matter as long as it is consistent?
- Mario: consistency is key.

Meeting Conclusions:

- Write up the results and analysis with references to the old code's results as a baseline for the new more efficient code with the new averaging mechanism.
- Jocelyn, Rishabh and Aileene should arrange to finish the poster and add the recommended kinematic diagram proposed by Mario.

Meeting End Time: 11:22.

Board Member Feedback:

- Group seems to have spread out work very well and worked equally.

Finances

The costs associated with carrying out this group's project are shown in the table below. Due to the nature of the project, there were no costs for equipment nor materials. The price of the poster was the only financial cost involved.

	Item	Price (£)
	Poster Printing	35.00
Total		35.00

Table C.1: Breakdown of finances for the project.

Health and Safety

D.1 Risk Assessments

Below is the risk assessment that was carried out for this project.

DocuSign Envelope ID: 2B478D84-A7D3-47A6-99A4-1BCFE33745C5

Project Risk Assessment Form

UCL

Project Title	Reconstruction of kinematics of events with missing energy using forward tagging at the LHC
Location of Experiment	Physics Building, University College, Gower St, London WC1E 6BT
Description of Experiment	Developing programming techniques to reconstruct the kinematics of W bosons using the measurement of forward protons.
Persons Involved	Ashik Rahman, Aileene Wang, Gurpriya Dhami, Jocelyn Japnanto, Joe George, Rishabh Lassen, Rishi Kalra, Swathi Nambiar
Supervisor / Board Member	Professor Mario Campanelli

Hazard Identification (state the hazards involved in the work. Consider **Chemicals, Radiation, LASERS** (an additional assessment will also be needed), the **environment, equipment, manual handling, electrical equipment, fire and explosion, disposal of waste**)

Display screen equipment:

- May cause eyestrain when screens are used for long periods of time.
- Blue light from screens may cause discomfort.

Electrical devices:

- Mains voltage may cause electric shock or pose a fire hazard.
- Charging cables and wires may cause a tripping hazard or devices falling onto experimenters.
- Liquid spillages may cause electric shocks or damage to electronics.
- Computers overheating, causing fire hazard.

Risk Assessment (assess the risks involved in the work and state high, medium or low risk)

riskNET Incident 6 x 5 risk matrix

Severity		Likelihood				
		Remote	Unlikely	Possible	Likely	Certain
Very	Non injury	A	A	A	A	A
	Minor injury	A	A	B	B	C
	Lost time injury, temporary disability or illness	A	B	C	C	D
	Permanent disability or major injury	B	C	C	D	D
	Fatality, multiple serious injuries/illnesses	C	C	D	D	D
	Multiple fatalities	C	D	D	D	D

A Very Low Risk - Initial Assessment
B Low Risk - Local Investigation
C Medium Risk - Local/Full Investigation
D High/Very High Risk - Full Investigation

Display screen equipment: A (Very Low Risk)
Electrical devices: A (Very Low Risk)

APPENDIX D. HEALTH AND SAFETY

DocuSign Envelope ID: 2B478D84-A7D3-47A6-99A4-1BCFE33745C5

Control Measures (say how you will reduce the risk to an acceptable level)

Display screen equipment:

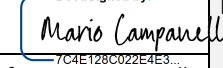
1. Take adequate breaks (e.g. 15 minutes per hour of work) to rest eyes

Electrical devices:

1. Keep lids on water bottles and clear up any spillages as they arise.
2. Keep charging cables away from each other to avoid tangling.
3. Turn off mains when not in use.
4. Ensure all electrical equipment tested annually to ensure electrical safety.

Declaration

I the undersigned have assessed the work, titled above, and declare that there is no significant risk / the risks will be controlled by the methods stated on this form and that the work will be carried out in accordance with Departmental codes of practice.

Assessor	Prof. Mario Campanelli	Date
Signature	 7C4E128C022E4E3...	06/02/2023
Supervisor/Board Member	Prof. Mario Campanelli	
Signature	 7C4E128C022E4E3...	06/02/23

Name	Signature
Rishi Kalra	 A91B3C89F0844B...
Joe George	 65A759C03F50450...
Aileene Wang	 Aileene Wang
Ashik Rahman	 A91B3C89F0844B...
Gurpriya Dhami	 DocuSigned by: Gurpriya Dhami
Rishabh Lassen	 Rishabh Lassen
Swathi Nambiar	 Swathi Nambiar
Jocelyn Japnanto	 Jocelyn Japnanto

D.2 Completion Certificates



Figure D.1: Rishabh Lassen: Completed and passed "Principles of Risk Assessment" on 12/01/2023



Figure D.2: Rishabh Lassen: Completed and passed "Principles of Laboratory Safety" on 12/01/2023



Figure D.3: Rishi Kalra: Completed and passed "Principles of Risk Assessment" on 13/01/2023



Figure D.4: Rishi Kalra: Completed and passed "Principles of Laboratory Safety" on 13/01/2023



Figure D.5: Gurpriya Dhami: Completed and passed "Principles of Risk Assessment" on 13/01/2023



Figure D.6: Gurpriya Dhami: Completed and passed "Principles of Laboratory Safety" on 13/01/2023



Figure D.7: Joe George: Completed and passed "Principles of Risk Assessment" on 13/01/2023



Figure D.8: Joe George: Completed and passed "Principles of Laboratory Safety" on 13/01/2023



Figure D.9: Swathi Nambiar: Completed and passed "Principles of Risk Assessment" on 12/01/2023



Figure D.10: Swathi Nambiar: Completed and passed "Principles of Laboratory Safety" on 12/01/2023



Figure D.11: Ai Wang: Completed and passed "Principles of Risk Assessment" on 13/01/2023



Figure D.12: Ai Wang: Completed and passed "Principles of Laboratory Safety" on 13/01/2023



Figure D.13: Ashik Rahman: Completed and passed "Principles of Risk Assessment" on 12/01/2023



Figure D.14: Ashik Rahman: Completed and passed "Principles of Laboratory Safety" on 12/01/2023



Figure D.15: Jocelyn Japnanto: Completed and passed "Principles of Risk Assessment" on 13/01/2023



Figure D.16: Jocelyn Japnanto: Completed and passed "Principles of Laboratory Safety" on 13/01/2023

Gantt Chart

As of March 17th, 2023, the Gantt chart snapshot below shows the progress of the project.

APPENDIX E. GANTT CHART

Project Name: Reconstruction of kinematics of events with missing energy using forward tagging at the LHC

Theory Team: Ai, Jocelyn, Priya, Ashik	Project Start:	Fri, 13/01/2023										
Code Team: Rishabh, Rishi, Joe, Swathi	Display Week:	1									9 Jan 2023	
TASK	ASSIGNED TO	PROGRESS	START	END	WORK DAYS	M	T	W	T	F	S	SMTW
Literature Review												
Kinematic reconstruction and WWREC research paper	Everyone	100%	13/1/23	27/1/23	14							
LHC and AFP detector physics	Ai, Jocelyn	100%	22/1/23	7/2/23	14							
W-boson leptonic decay and particle physics	Priya, Ashik	100%	22/1/23	7/2/23	14							
Computational research (C/C++ efficiency)	Code Team	100%	4/2/23	18/2/23	14							
Preliminary Work												
C++, ROOT installation and tutorials	Code Team	100%	9/2/23	18/2/23	7							
Testing the reconstruction source code	Code Team	100%	9/2/23	18/2/23	7							
Adjusting the plotting code (dps.C) parameters	Code Team	100%	9/2/23	18/2/23	7							
Code Efficiency												
Removing variable redundancies	Code Team	100%	16/2/23	23/2/23	7							
Replacing inefficient variable structures	Code Team	100%	16/2/23	23/2/23	7							
Implementing automatic looping	Joe	100%	16/2/23	23/2/23	7							
Enabling recording of parameter information	Joe	100%	23/2/23	2/3/23	7							
Increasing rapidity through functions and looping structures	Joe	100%	23/2/23	2/3/23	7							
Code Optimisation												
Optimisation of modifiable parameters	Joe	100%	23/2/23	2/3/23	7							
Substituting in new averaging mechanism	Joe	100%	23/2/23	2/3/23	7							
Investigating parallel coding and clustering	Joe, Rishabh	100%	26/2/23	8/3/23	10							
Testing with proton smearing	Joe, Swathi	100%	6/3/23	13/3/23	10							
Collecting results and performing analysis	Code Team	100%	6/3/23	13/3/23	7							
Final Report Write-Up												
Background	Rishi	100%	10/2/23	24/2/23	14							
Report formatting and layout	Joe, Rishi, Rishabh	100%	10/2/23	24/2/23	14							
Theory: ATLAS & AFP detector	Ai, Jocelyn	100%	21/2/23	28/2/23	7							
Theory: Standard Model and Effective Field Theory	Ashik	100%	24/2/23	3/3/23	7							
Theory: W Boson decay and particle physics	Rishi	100%	24/2/23	3/3/23	7							
Method: Code optimisation	Joe, Priya	100%	3/3/23	10/3/23	7							
Results and analysis	Code Team	100%	3/3/23	10/3/23	7							
Conclusion and future improvements	Everyone	100%	10/3/23	15/3/23	5							
Appendices	Rishabh, Rishi	100%	10/3/23	17/3/23	7							
Executive Summary + Editing	Everyone	100%	10/3/23	17/3/23	7							
Poster Creation												
Poster design and layout	Jocelyn, Rishabh, Swathi	100%	10/3/23	17/3/23	7							
Poster images and content	Rishi, Rishabh, Swathi	100%	10/3/23	17/3/23	7							
Poster printing	Swathi	100%	10/3/23	17/3/23	7							
<i>Insert new rows ABOVE this one</i>												

Figure E.1: Gantt Chart 1

APPENDIX E. GANTT CHART

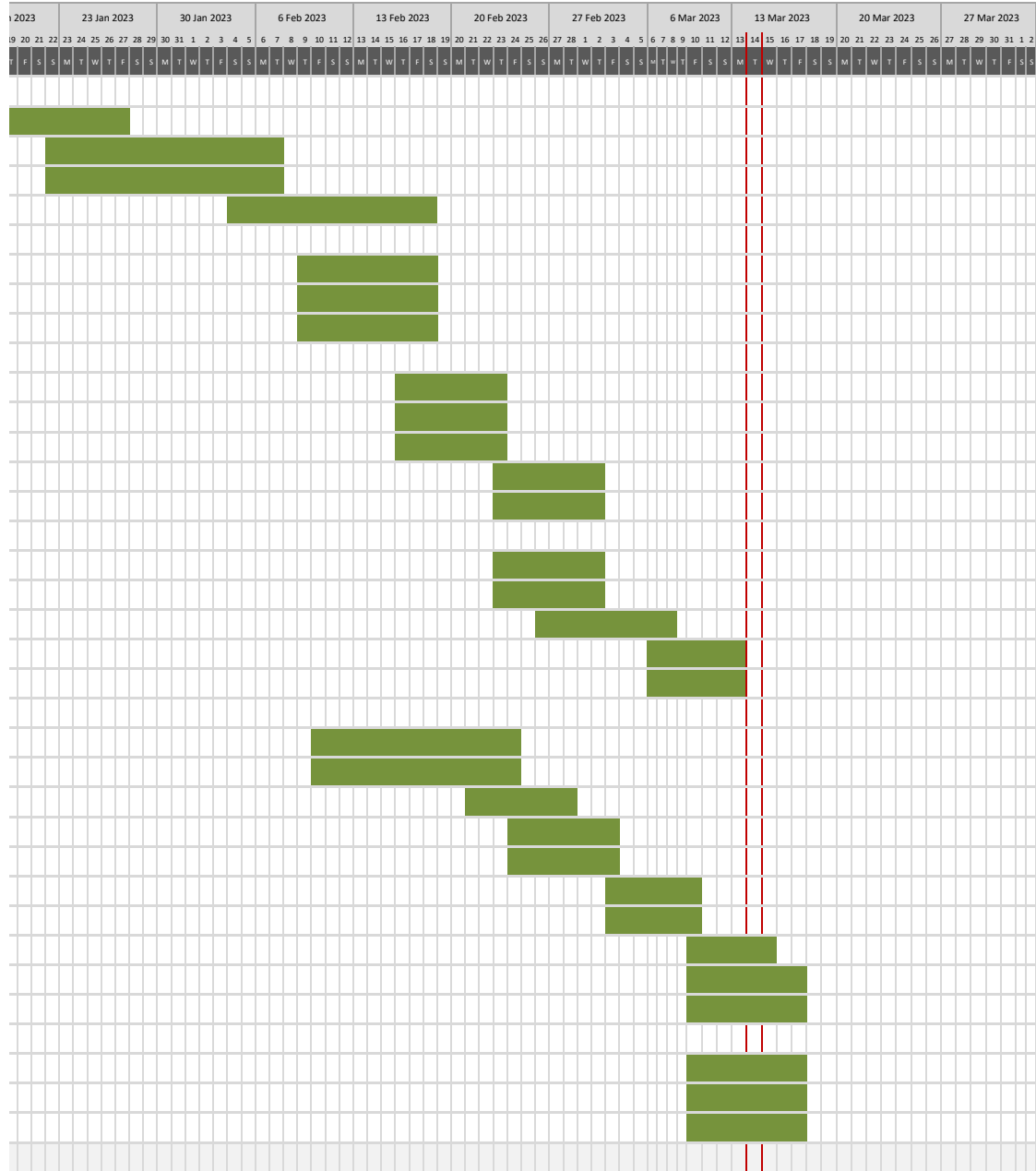


Figure E.2: Gantt Chart 2